

# Dynamical Functions of a 1D Correlated Quantum Liquid

J. M. P. Carmelo<sup>1</sup>, D. Bozi<sup>2</sup> and K. Penc<sup>3</sup>

<sup>1</sup>GCEP-Center of Physics, U. Minho, Campus Gualtar, P-4710-057 Braga, Portugal

<sup>2</sup>Centro de Física de Materiales, Centro Mixto CSIC-UPV/EHU, E-20018 San Sebastian, Spain

<sup>3</sup>Res. Inst. for Solid State Physics and Optics, H-1525 Budapest, P.O.B. 49, Hungary  
E-mail: carmelo@fisica.uminho.pt

**Abstract.** The dynamical correlation functions in the one-dimensional electronic systems show power-law behavior at low energies and momenta close to integer multiples of the charge and spin *Fermi momenta*. These systems are usually referred to as Tomonaga-Luttinger liquids. However, near well-defined lines of the  $(k, \omega)$  plane the power-law behaviour extends beyond the low-energy cases mentioned above, and also appears at higher energies leading to singular features in the photoemission spectra and other dynamical correlation functions. The general spectral-function expressions derived in this paper were used in recent theoretical studies of the finite-energy singular features in photoemission of the organic compound tetrathiafulvalene-tetracyanoquinodimethane (TTF-TCNQ) metallic phase. They are based on a so called pseudofermion dynamical theory (PDT), which allows us to systematically enumerate and describe the excitations in the Hubbard model starting from the Bethe-Ansatz, as well as to calculate the charge and spin objects phase shifts appearing as exponents of the power laws. In particular, we concentrate on the spin-density  $m \rightarrow 0$  limit and in effects of the vicinity of the singular border lines, as well as close to half filling. Our studies take into account spectral contributions from types of microscopic processes that do not occur for finite values of the spin density. In addition, the specific processes involved in the spectral features of TTF-TCNQ are studied. Our results are useful for the further understanding of the unusual spectral properties observed in low-dimensional organic metals and also provide expressions for the one- and two-atom spectral functions of a correlated quantum system of ultracold fermionic atoms in a 1D optical lattice with on-site two-atom repulsion.

PACS numbers: 71.00

## 1. INTRODUCTION

The low-energy physics of correlated one-dimensional (1D) problems has some universal properties described by the Tomonaga-Luttinger liquid (TLL) [1]. In turn, a pseudofermion dynamical theory (PDT) beyond the TLL [2, 3] was recently used to study the finite-energy singular features in photoemission of the organic compound tetrathiafulvalene-tetracyanoquinodimethane (TTF-TCNQ) metallic phase [4]. While the PDT was originally introduced for the 1D Hubbard model, more recently other methods for the study of finite-energy spectral and dynamical functions of 1D correlated systems were introduced [5, 6]. Both the finite-energy spectral-weight distributions studied by the PDT for the 1D Hubbard model and the methods of Refs. [5, 6] for other 1D correlated problems include power-law singularities near well-defined branch lines with exponents depending on the interaction strength and the excitation momentum. In the limit of low energy the PDT correlation- and spectral-function expressions recover the usual low-energy TLL results [7]

Besides a renewed interest in the unusual spectral and dynamical properties of quasi-1D organic compounds [8, 9], recently there has been an increasing interest in those of interacting ultracold fermionic atoms in 1D optical lattices [10]. Quantum effects are strongest at low dimensionality leading to unusual phenomena such as charge-spin separation at all energies [8, 9]. Thus, the further understanding of the microscopic mechanisms behind the unusual spectral properties observed in low-dimensional correlated systems and materials is a topic of high scientific interest.

The 1D Hubbard model is one of the few realistic models for correlated electrons in a discrete lattice for which one can exactly calculate all the energy eigenstates and their energies [11, 12, 13]. It includes a first-neighbor transfer-integral  $t$ , for electron hopping along the chain, and an effective on-site Coulomb repulsion  $U$ . For finite-energy values the metallic phase of this model goes beyond the low energy behavior described by the usual TLL [1] and thus the study of spectral functions is a very involved many-electron problem. Fortunately, the construction of a pseudofermion description by means of a unitary transformation which slightly shifts the discrete momentum values of the corresponding pseudoparticles of Refs. [14, 15] leads to the PDT, whose energy spectrum has no residual-interaction energy terms. Therefore, such a description is suitable for the derivation of explicit expressions for these functions [2, 3, 7].

The PDT is a generalization for finite values of  $U$  of the scheme introduced in Refs. [16, 17] for large  $U$  values. It profits from the use of a description of the exact energy eigenstates in terms of occupancy configurations of several branches of pseudofermions. The ground state has finite occupancy of charge  $c$  and spin  $s_1$  pseudofermions only. Under the ground-state - excited-energy-eigenstate transitions, the pseudofermions and pseudofermion holes undergo elementary scattering events with the pseudofermions and pseudofermion holes created in these transitions. This leads to excited-state, interaction, density, and two-momenta dependent two-pseudofermion phase shifts. The point is that the one- and two-electron spectral functions can be expressed in terms of pseudofermion

determinants which are a functional of such phase shifts. Use of the PDT reveals that for finite values of  $U/t$  all singular one-electron spectral features of the model are of power-low type, controlled by negative exponents. Furthermore, the PDT line shapes associated with such exponents were found to correspond to the unusual charge and spin spectral features observed by photoemission experiments for the whole finite-energy band width in quasi-1D organic metals [18]. (The use of the Dynamical Density Matrix Renormalization Group method [19] leads to results consistent with those obtained by the PDT.) Furthermore, when combined with the Renormalization Group, the use of the PDT reveals that a system of weakly coupled Hubbard chains is suitable for the successful description of the phase diagram observed in quasi-1D doped Mott-Hubbard insulators [20].

The low-energy physics of the model corresponds to the universal TLL behaviour and was studied by different techniques, such as conformal-field theory [21] and bosonization [22]. There are many investigations where the low-energy conformal invariance was combined with the model exact Bethe-ansatz solution in the study of the asymptotics of correlation functions and related quantities [1, 22]. As mentioned above, the studies of Ref. [7] confirm that in the limit of low energy the general finite-energy spectral and correlation function expressions provided by the PDT in Ref. [2] recover the correct behaviour given by conformal-field theory.

The main goal of this paper is to provide the details of an extension of the PDT introduced in Refs. [2, 3, 7] to initial ground states with spin density  $m \rightarrow 0$  which was used in recent theoretical studies of the finite-energy singular features in photoemission of the TTF-TCNQ metallic phase [4]. The point is that such an extension involves spectral contributions that do not occur for finite values of the spin density and hence are not taken into account by the expressions of Refs. [2, 3, 7]. In order to introduce the generalized spectral-function expressions used in the recent studies of the TTF-TCNQ spectral features presented in short form in Ref. [4] we present here such an extension of the PDT.

The unusual spectral properties are mainly determined by the occupancy configurations in the excited states of the two pseudofermion branches that have finite occupancies for the ground state. Those are the charge  $c0$  pseudofermion and spin  $s1$  pseudofermion branches. The ground-state corresponds to charge  $c0$  pseudofermion (and spin  $s1$  pseudofermion) finite occupancy for canonical-momentum values in the range  $|\bar{q}| < q_{Fc0}^0 = 2k_F$  (and  $|\bar{q}| < q_{Fs1}^0 = k_{F\downarrow}$ ) and charge  $c0$  pseudofermion-hole (and spin  $s1$  pseudofermion-hole) finite occupancy for canonical-momentum values in the range  $2k_F < |\bar{q}| < q_{c0}^0 = \pi$  (and  $k_{F\downarrow} < |\bar{q}| < q_{s1}^0 = k_{F\uparrow}$ ). The values of the four deviations  $\Delta\bar{q}_{Fc0,\pm 1}$  and  $\Delta\bar{q}_{Fs1,\pm 1}$  in the two charge  $\pm q_{Fc0}^0 = \pm 2k_F$  and two spin  $\pm q_{Fs1}^0 = \pm k_{F\downarrow}$  *Fermi* points under each ground-state - excited-energy-eigenstate transition play a major role in the PDT.

We denote such deviations by  $\Delta\bar{q}_{F\alpha\nu,\iota}$  where  $\alpha\nu = c0, s1$  and  $\iota = \pm 1$ . The spectral-weight distributions are controlled by the values of the following associated

four parameters,

$$2\Delta_{\alpha\nu}^{\iota} = \left( \frac{\Delta \bar{q}_{F\alpha\nu,\iota}}{[2\pi/L]} \right)^2 ; \quad \alpha\nu = c0, s1 ; \quad \iota = \pm 1, \quad (1)$$

where  $L \gg 1$  is the 1D lattice length within the use of periodic boundary conditions. According to the PDT, the contributions from ground-state transitions to subspaces spanned by sets of excited energy eigenstates with the same values for the two charge parameters  $2\Delta_{c0}^{\pm 1}$  and two spin parameters  $2\Delta_{s1}^{\pm 1}$  fully determine the momentum  $k$  and energy  $\omega$  dependence of the general finite-energy spectral functions in the small  $(k, \omega)$ -plane region associated with the energy and momentum spectrum of these excited states [2, 3].

The general PDT finite-energy spectral-function expressions given in Ref. [2] refer to the metallic phase for initial ground states with spin densities  $m$  in the range  $0 < m < n$ , where  $n$  is the electronic density such that  $0 < n < 1$ . Actually, the expressions found in Ref. [2] refer to values of  $n$  such that the *Fermi*-point charge velocity  $v_{c0}$  is larger than the *Fermi*-point spin velocity  $v_{s1}$ . For finite values of  $U/t$ , this excludes densities  $n$  in the vicinity of half filling. One of our goals is to extend the studies of that reference to electronic densities such that  $v_{s1} > v_{c0}$ .

The general expressions of the exponents that control the singular features of the above finite-energy spectral function expressions provide the correct zero spin-density values in the limit  $m \rightarrow 0$ . Moreover, as given in Eq. (55) of Ref. [2], for excitations such that  $2\Delta_{\alpha\nu}^{\iota} \neq 0$  for the two  $\alpha\nu = c0$  charge and two  $\alpha\nu = s1$  spin parameters, the corresponding four pseudofermion relative weights have the asymptotic expression provided in that equation. It follows that for zero-spin excitations such that the four parameters  $2\Delta_{\alpha\nu}^{\iota}$  where  $\alpha\nu = c0, s1$  and  $\iota = \pm 1$  are finite, the general convolution function and corresponding pre-factor function  $F_0(z)$  given in Eqs. (61) and (62) of Ref. [2], respectively, provide the correct zero spin-density contributions to the spectral-function expressions in the limit of zero spin density. The point is that for densities in the ranges  $0 < n < 1$  and  $0 < m < n$  all ground-state - excited-energy-eigenstate transitions lead to finite values for these four parameters.

While some  $m \rightarrow 0$  one- and two-electron excitations also lead to finite values for the two  $\alpha\nu = c0$  charge and two  $\alpha\nu = s1$  spin parameters  $2\Delta_{\alpha\nu}^{\iota}$ , there are also  $m \rightarrow 0$  excitations for which one (or both) spin parameter(s)  $2\Delta_{s1}^{\pm 1}$  vanishes (or vanish). In that case the corresponding  $s1, \iota$  pseudofermion relative weights have not the asymptotic expression provided in Eq. (55) of Ref. [2]. Nonetheless, we find in this paper that the contributions to the spectral-function expressions from ground-state transitions to the excited energy eigenstates which span such excitations lead to convolution functions of the same general form as that provided in Eq. (61) of Ref. [2]. The only difference is that the pre-factor  $F_0(z)$  of such convolution functions given in Eq. (62) of that reference is replaced by another suitable function derived in this paper and given in Appendix A.

Since these convolution functions fully control all the different spectral-function contributions given in Eqs. (66), (68), and (70) of Ref. [2], the derivation of all  $m = 0$  contributions requires the use of such suitable pre-factors, which were taken into account

in the studies of the TTF-TCNQ spectral features of Ref. [4] and we calculate in this paper. Interestingly, the different expressions found here for the pre-factor  $F_0(z)$  are such that the corresponding pre-factors of the space and time asymptotic expressions of correlation functions [7] are continuous functions of  $m$  as  $m \rightarrow 0$ .

The extension of the expressions for the one- and two-electron spectral-weight distributions introduced in Ref. [2] for the 1D Hubbard model to the regime where  $m \rightarrow 0$  involves taking into account contributions from transitions to subspaces spanned by excited states such that one, two, three, or even four out of the four parameters  $2\Delta_{\alpha\nu}^{\iota}$  where  $\alpha\nu = c0, s1$  and  $\iota = \pm 1$  vanish. Note that according to Eq. (1), the value of the  $\alpha\nu, \iota$  pseudofermion canonical-momentum *Fermi* points associated with  $2\Delta_{\alpha\nu}^{\iota} = 0$  values remains unchanged under the corresponding ground-state - excited-state transitions. Such contributions do not exist for the  $m > 0$  regime addressed in Ref. [2] but must be taken into account in the quantitative study of the spectral-weight distributions of the correlated metal at zero spin density. In this paper we also extend the one- and two-electron spectral-weight distributions of Ref. [2] to all electronic densities of the metallic phase. Although we do not consider the half-filling Mott-Hubbard insulator such that  $v_{c0} = 0$ , our expressions refer to all electronic densities of the metallic phase and thus also for those in the vicinity of 1.

Another problem solved in this paper is the derivation of explicit expressions for the spectral functions in the vicinity of the singular border lines, which again were used in the recent studies of the TTF-TCNQ spectral features of Ref. [4]. For that one-electron problem such border lines correspond to processes for which the extra charge and spin objects created upon removal or addition of the electron have exactly the same velocity. Such an equality of the charge and spin velocities occurs at well-defined lines in the  $(k, \omega)$  plane and leads to power-law singular behavior along such a border lines. In contrast to the power-law branch-line singular features studied in Ref. [2], which are controlled by momentum,  $U/t$ , and density dependent negative exponents, the border-line power-law singular features are controlled by an universal exponent given by  $-1/2$ , as given in Eq. (2) of Ref. [4]. Further details on the processes involved in the applications to TTF-TCNQ are also reported.

The paper is organized as follows: In Sec. 2 we introduce the model and provide basic information about the pseudofermion description needed for our studies. In Sec. 3 the general expressions required for the study of the finite-energy spectral-weight distributions of the metallic phase for initial  $m \rightarrow 0$  ground states are calculated. That includes derivation of explicit expressions of the spectral functions in the vicinity of the singular border lines for density ranges  $0 < n < 1$  and  $0 \leq m < n$ . In Sec. 4 we use the expressions obtained in the previous section and in Ref. [2] to provide further details on the processes that contribute to the unusual photoemission spectrum of TTF-TCNQ. Finally, the concluding remarks are presented in Sec. 5.

## 2. THE PROBLEM AND THE PSEUDOFERMION DESCRIPTION

Our study focus on finite- $\omega$   $\mathcal{N}$ -electron spectral-weight distributions of the following general form,

$$B_{\mathcal{N}}^l(k, \omega) = \sum_f |\langle f | \hat{O}_{\mathcal{N}}^l(k) | GS \rangle|^2 \delta(\omega - l[E_f - E_{GS}]); \quad l\omega > 0, \quad (2)$$

where  $l = \pm 1$ . We focus our attention on the cases of more physical interest which correspond to  $\mathcal{N} = 1, 2$ . In the above expression the general  $\mathcal{N}$ -electron operators  $\hat{O}_{\mathcal{N}}^{+1}(k) \equiv \hat{O}_{\mathcal{N}}^{\dagger}(k)$  and  $\hat{O}_{\mathcal{N}}^{-1}(k) \equiv \hat{O}_{\mathcal{N}}(k)$  carry momentum  $k$ , the  $f$  summation runs over the excited energy eigenstates, the energy  $E_f$  corresponds to these states, and  $E_{GS}$  is the initial ground-state energy. The local operator  $\hat{O}_{\mathcal{N},j}^{+1} \equiv \hat{O}_{\mathcal{N},j}^{\dagger}$  or  $\hat{O}_{\mathcal{N},j}^{-1} \equiv \hat{O}_{\mathcal{N},j}$  is related to the corresponding momentum-representation operator  $\hat{O}_{\mathcal{N}}^l(k)$  of Eq. (2) by a Fourier transform. As in Ref. [2], we use in expression (2) a momentum extended scheme such that  $k \in (-\infty, +\infty)$ .

We consider weight distributions (2) that refer to the Hubbard model in a 1D lattice with periodic boundary conditions and units such that the Planck constant and electronic lattice constant are one,

$$\hat{H} = -t \sum_{j,\sigma} [c_{j,\sigma}^{\dagger} c_{j+1,\sigma} + h.c.] + U \sum_j \hat{n}_{j,\uparrow} \hat{n}_{j,\downarrow}. \quad (3)$$

Here  $c_{j,\sigma}^{\dagger}$  (and  $c_{j,\sigma}$ ) creates (and annihilates) one spin-projection  $\sigma = \uparrow, \downarrow$  electron at site  $j = 1, 2, \dots, N_a$  and  $\hat{n}_{j,\sigma} = c_{j,\sigma}^{\dagger} c_{j,\sigma}$ . Let  $N = N_{\uparrow} + N_{\downarrow}$  be the electronic number,  $N_a$  the number of lattice sites, and  $n_{\sigma} = N_{\sigma}/L = N_{\sigma}/N_a$ .  $N_a$  is assumed to be even and very large. The electronic densities  $n = n_{\uparrow} + n_{\downarrow}$  and spin densities  $m = n_{\uparrow} - n_{\downarrow}$  are in the ranges  $0 < n < 1$  and  $0 \leq m < n$ , respectively. Except for corrections of order of  $1/L$ , the Fermi momenta are given by  $k_F = \pi n/2$  and  $k_{F\sigma} = \pi n_{\sigma}$ .

The concept of a rotated electron plays a key role in the pseudofermion description. Concerning its relation to the holons, spinons, and  $c0$  pseudoparticles whose occupancy configurations describe the energy eigenstates of the model (3), see Ref. [14]. Our studies do not involve directly the holons and spinons as defined in that reference. The charge  $c\nu$  pseudofermions (and spin  $s\nu$  pseudofermions) such that  $\nu = 1, 2, 3, \dots$  are  $2\nu$ -holon (and  $2\nu$ -spinon) composite quantum objects whose discrete momentum values are slightly shifted relative to those of the corresponding  $c\nu$  pseudoparticles (and spin  $s\nu$  pseudoparticles) studied in Refs. [14, 15]. Such momentum shifts cancel exactly the residual-interaction terms of the pseudoparticle energy spectrum. Otherwise, pseudoparticles and pseudofermions have the same properties.

According to the PDT of Refs. [2, 7], the charge  $c0$  pseudofermions and spin  $s1$  pseudofermions play the major role in the spectral properties. The holons (and spinons) which are not part of  $2\nu$ -holon composite  $c\nu$  pseudofermions (and  $2\nu$ -spinon composite  $s\nu$  pseudofermions) are the Yang holons (and HL spinons). Those are invariant under the electron - rotated-electron unitary transformation and hence have a non-interacting character and do not contribute to the matrix elements between energy eigenstates

of the spectral-weight distributions studied in this paper. We denote the numbers of  $\alpha\nu$  pseudofermions and  $\alpha\nu$  pseudofermion holes by  $N_{\alpha\nu}$  and  $N_{\alpha\nu}^h$ , respectively, where  $\alpha = c, s$  and  $\nu = 0, 1, 2, \dots$  for  $\alpha = c$  and  $\nu = 1, 2, \dots$  for  $\alpha = s$ . (The value of  $N_{\alpha\nu}^h$  is given in Eqs. (B7) and (B8) of Ref. [14].)

Alike in Ref. [2], we use in this paper the notation  $\alpha\nu \neq c0, s1$  branches, which refers to all  $\alpha\nu$  branches except the  $c0$  and  $s1$  branches. Moreover, the summations (and products)  $\sum_{\alpha\nu}$ ,  $\sum_{\alpha\nu=c0, s1}$ , and  $\sum_{\alpha\nu \neq c0, s1}$  (and  $\prod_{\alpha\nu}$ ,  $\prod_{\alpha\nu=c0, s1}$ , and  $\prod_{\alpha\nu \neq c0, s1}$ ) run over all  $\alpha\nu$  branches with finite  $\alpha\nu$  pseudofermion occupancy in the corresponding state or subspace, the  $c0$  and  $s1$  branches only, and all  $\alpha\nu$  branches with finite  $\alpha\nu$  pseudofermion occupancy in the corresponding state or subspace except the  $c0$  and  $s1$  branches, respectively.

The pseudofermion description refers to a Hilbert subspace called the *pseudofermion subspace* (PS) in Ref. [2], in which the  $\mathcal{N}$ -electron excitations  $\hat{O}_{\mathcal{N}}^l(k)|GS\rangle$  are contained. The PS is spanned by the initial ground state and the excited energy eigenstates originated from it by creation, annihilation, and particle-hole processes involving the generation of a finite number of active pseudofermion scattering centers, Yang holons, and HL spinons plus a vanishing or small density of low-energy and small-momentum  $\alpha\nu = c0, s1$  pseudofermion particle-hole processes. It is convenient to classify these processes into three types, called processes (A), (B), and (C), as further discussed in the ensuing section.

The  $\alpha\nu$ -pseudofermion discrete canonical-momentum values have a functional character and read,  $\bar{q}_j = q_j + Q_{\alpha\nu}^{\Phi}(q_j)/L = [2\pi/L]I_j^{\alpha\nu} + Q_{\alpha\nu}^{\Phi}(q_j)/L$  where  $j = 1, 2, \dots, N_{\alpha\nu}^*$  and  $N_{\alpha\nu}^* = N_{\alpha\nu} + N_{\alpha\nu}^h$ . Here is a  $Q_{\alpha,\nu}^{\Phi}(q_j)/2$  is a  $\alpha\nu$  pseudofermion scattering phase shift given by,

$$Q_{\alpha\nu}^{\Phi}(q_j)/2 = \sum_{\alpha'\nu'}^{N_{\alpha'\nu'}^*} \sum_{j'=1}^{N_{\alpha'\nu'}^*} \pi \Phi_{\alpha\nu, \alpha'\nu'}(q_j, q_{j'}) \Delta N_{\alpha'\nu'}(q_{j'}); \quad j = 1, 2, \dots, N_{\alpha\nu}^*, \quad (4)$$

where  $\Delta N_{\alpha\nu}(q_j) = \Delta \mathcal{N}_{\alpha\nu}(\bar{q}_j)$  is the bare-momentum distribution function deviation  $\Delta N_{\alpha\nu}(q_j) = N_{\alpha\nu}(q_j) - N_{\alpha\nu}^0(q_j)$  corresponding to the excited energy eigenstate. This deviation is expressed in terms of the *bare-momentum*  $q_j = [2\pi I_j^{\alpha\nu}]/L$ , which is carried by the  $\alpha\nu$  pseudoparticles, where  $I_j^{\alpha\nu}$  are the quantum numbers provided by the Bethe-ansatz solution [14].

Although the  $\alpha\nu$  pseudoparticles carry bare-momentum  $q_j$ , one can also label the corresponding  $\alpha\nu$  pseudofermions by such a bare-momentum. When we refer to the pseudofermion bare-momentum  $q_j$ , we mean that  $q_j$  is the bare-momentum value that corresponds to the pseudofermion canonical momentum  $\bar{q}_j = q_j + Q_{\alpha\nu}^{\Phi}(q_j)/L$ . For the ground state the pseudofermion numbers are given by  $N_{c0} = N$ ,  $N_{s1} = N_{\downarrow}$ ,  $N_{\alpha\nu} = 0$  for  $\alpha\nu \neq c0, s1$ . We call  $N_{c0}^0$  and  $N_{s1}^0$  the ground-state  $c0$  and  $s1$  pseudofermion numbers, respectively. As mentioned in the previous section, the ground-state  $\alpha\nu = c0, s1$  bare-momentum distribution functions are such that there is pseudofermion occupancy for  $|q| \leq q_{F\alpha\nu}^0$  and unoccupancy for  $q_{F\alpha\nu}^0 < |q| \leq q_{\alpha\nu}^0$ , where in the thermodynamic limit

the *Fermi-point* values are given by,

$$q_{F_{c0}}^0 = 2k_F; \quad q_{F_{s1}}^0 = k_{F\downarrow}. \quad (5)$$

Moreover, for that state the limiting bare-momentum values of both the  $\alpha\nu = c0, s1$  and  $\alpha\nu \neq c0, s1$  bands read,

$$q_{c0}^0 = \pi; \quad q_{s1}^0 = k_{F\uparrow}; \quad q_{c\nu}^0 = [\pi - 2k_F], \quad \nu > 0; \quad q_{s\nu}^0 = [k_{F\uparrow} - k_{F\downarrow}], \quad \nu > 1. \quad (6)$$

The ground-state  $\alpha\nu = c0, s1$  densely-packed bare-momentum distribution functions  $N_{\alpha\nu}^0(q_j)$  are given in Eqs. (C.1)-(C.3) of Ref. [14].

Under the ground-state - excited-energy-eigenstate transitions, the  $\alpha\nu$  pseudofermions and  $\alpha\nu$  pseudofermion holes undergo elementary scattering events with the  $\alpha'\nu'$  pseudofermions and  $\alpha'\nu'$  pseudofermion holes created in these transitions [2]. This leads to the elementary two-pseudofermion phase shifts  $\pi \Phi_{\alpha\nu, \alpha'\nu'}(q_j, q_{j'})$  on the right-hand side of the overall scattering phase shift (4), as further discussed in Ref. [23]. Moreover, within the PDT the overall  $\alpha\nu$  pseudofermion or hole phase shift,

$$Q_{\alpha\nu}(q_j)/2 = Q_{\alpha\nu}^0/2 + Q_{\alpha\nu}^\Phi(q_j)/2, \quad (7)$$

controls the spectral weight distributions. Here  $Q_{\alpha\nu}(q_j)/L$  gives the shift in the discrete canonical-momentum value  $\bar{q}_j$  that arises due to the transition from the ground state to an excited energy eigenstate and  $Q_{\alpha\nu}^0/2$  can have the values  $Q_{\alpha\nu}^0/2 = 0, \pm\pi/2$  [2, 23]. In this paper we use boundary conditions such that  $Q_{\alpha\nu}^0/2 = 0, -\text{sgn}(k)\pi/2$ , where  $k$  is the excited-state momentum relative to that of the initial ground state. Here we assume that for the latter state  $N/2$  and  $N$  are odd and even numbers, respectively.  $Q_{\alpha\nu}^0/L$  gives the shift in the discrete bare-momentum value  $q_j$  that arises as a result of the same transition.

The  $\alpha\nu$  pseudofermion creation and annihilation operators  $f_{\bar{q}_j, \alpha\nu}^\dagger$  and  $f_{\bar{q}_j, \alpha\nu}$ , respectively, have exotic anticommutation relations [2]. These anticommutators involve the overall phase shifts (7) and play a key role in the spectral properties. There are corresponding local operators  $f_{x_j, \alpha\nu}^\dagger$  and  $f_{x_j, \alpha\nu}$ . Here  $x_j$  where  $j = 1, 2, \dots, N_{\alpha\nu}^*$  are the spatial coordinates of a  $\alpha\nu$  effective lattice with  $N_{\alpha\nu}^*$  sites. Each of the  $N_{\alpha\nu}$  occupied sites of such a lattice correspond to well-defined occupancy configurations of  $2\nu$  sites of the rotated-electron lattice. It turns out that the operators  $f_{x_j, \alpha\nu}^\dagger$  and  $f_{x_j, \alpha\nu}$  have simple anticommutation relations. Indeed, the exotic anticommutation relations of the operators and  $f_{\bar{q}_j, \alpha\nu}^\dagger$  and  $f_{\bar{q}_j, \alpha\nu}$  result from the form of the discrete canonical momentum values  $\bar{q}_j = q_j + Q_{\alpha\nu}^\Phi(q_j)/L = [2\pi/L]I_j^{\alpha\nu} + Q_{\alpha\nu}^\Phi(q_j)/L$ .

There is a simple relation between the  $f_{x_j, c0}^\dagger$  and  $f_{x_j, c0}$  operators and those of the rotated electrons such that the former operators have anticommutation relations. To show that for branches  $\alpha\nu \neq c0$  the operators  $f_{x_j, \alpha\nu}^\dagger$  and  $f_{x_j, \alpha\nu}$  also have anticommutation relations is a much more involved problem. The composite  $\alpha\nu \neq c0$  pseudofermions emerge from from corresponding  $\alpha\nu \neq c0$  bond particles through a suitable Jordan-Wigner transformation [24]. The point is that such  $\alpha\nu \neq c0$  bond particles live on the corresponding  $\alpha\nu$  effective lattice and behave there as hard-core bosons. That interesting problem will be studied in detail elsewhere.

The charge and spin pseudofermion *Fermi*-point group velocities  $v_{c0}$  and  $v_{s1}$  also play an important role in our study. The velocity  $v_{\alpha\nu}$  with  $\alpha\nu = c0, s1$  is a particular case of the momentum-dependent group velocity  $v_{\alpha\nu}(q)$ . Such velocities appear in all the spectral-weight distribution expressions of the metallic phase and are given by,

$$v_{\alpha\nu}(q) = \frac{\partial \epsilon_{\alpha\nu}(q)}{\partial q}, \quad \text{all branches}; \quad v_{\alpha\nu} \equiv v_{\alpha\nu}(q_{F\alpha\nu}^0), \quad \alpha\nu = c0, s1. \quad (8)$$

In the first expression  $\epsilon_{\alpha\nu}(q)$  stands for the  $\alpha\nu$  pseudofermion energy dispersion defined by Eqs. (18)-(20) of Ref. [2]. In this paper and its Appendix A we use often a convention according to which the  $\bar{\alpha}\bar{\nu} = c0, s1$  branch is that whose pseudofermion *Fermi*-point group velocity  $v_{\bar{\alpha}\bar{\nu}}$  is such that,

$$v_{\bar{\alpha}\bar{\nu}} = \min \{v_{c0}, v_{s1}\}. \quad (9)$$

### 3. SPECTRAL-WEIGHT DISTRIBUTIONS FOR THE METALLIC PHASE AND $0 \leq m < n$

#### 3.1. General spectral-function expressions

The pseudofermion elementary processes that generate the PS from the initial ground state belong to three types:

(A) Finite-energy and finite-momentum elementary  $c0$  and  $s1$  pseudofermion processes away from the corresponding *Fermi points* involving creation or annihilation of a finite number of pseudofermions plus creation of  $\alpha\nu \neq c0, s1$  pseudofermions with bare-momentum values different from the limiting bare-momentum values  $\pm q_{\alpha\nu}^0$ ;

(B) Zero-energy and finite-momentum processes that change the number of  $c0$  and  $s1$  pseudofermions at the  $\iota = \text{sgn}(q) 1 = +1$  right and  $\iota = \text{sgn}(q) 1 = -1$  left  $c0$  and  $s1$  *Fermi points* - these processes transform the ground-state densely packed bare-momentum occupancy configuration into an excited-state densely packed bare-momentum occupancy configuration. Furthermore, creation of a finite number of independent  $-1/2$  holons and independent  $-1/2$  spinons, including  $-1/2$  Yang holons,  $-1/2$  HL spinons, and  $-1/2$  holons and  $-1/2$  spinons associated with  $c\nu$  pseudofermions of limiting bare momentum  $q = \pm q_{c\nu}^0 = \pm[\pi - 2k_F]$  and  $s\nu$  pseudofermions of limiting bare momentum  $q = \pm q_{s\nu}^0 = \pm[k_{F\uparrow} - k_{F\downarrow}]$ , respectively;

(C) Low-energy and small-momentum elementary  $c0$  and  $s1$  pseudofermion particle-hole processes in the vicinity of the  $\iota = \text{sgn}(q) 1 = +1$  right and  $\iota = \text{sgn}(q) 1 = -1$  left  $c0$  and  $s1$  *Fermi points*, relative to the excited-state  $\alpha\nu = c0, s1$  pseudofermion densely packed bare-momentum occupancy configurations generated by the above elementary processes (B).

Such processes generate excitations which can be classified by the values of a set of numbers and number deviations. For instance,  $N_{\alpha\nu}^{phNF}$  is the number of finite-momentum and finite-energy  $\alpha\nu = c0, s1$  pseudofermion particle-hole processes of type

(A). The quantum number  $\iota = \text{sgn}(q)1 = \pm 1$  refers to the right pseudfermion movers ( $\iota = +1$ ) and left pseudfermion movers ( $\iota = -1$ ) and  $\Delta N_{\alpha\nu, \iota}^F$ , such that  $\Delta N_{\alpha\nu, \pm 1}^F$  is the deviation in the number of  $\alpha\nu$  pseudofermions at the right (+1) and left (-1) *Fermi points* generated by the elementary processes (B). In turn, the deviation in the number of  $\alpha\nu = c0, s1$  pseudofermions created or annihilated away from these points by the elementary processes (A) is denoted by  $\Delta N_{\alpha\nu}^{NF}$ .

The actual number of  $\alpha\nu$  pseudofermions created or annihilated at the right (+1) and left (-1) *Fermi points* by the processes (B) is denoted by  $\Delta N_{\alpha\nu, \pm 1}^{0,F}$ . It is such that  $\Delta N_{\alpha\nu, \iota}^F = \Delta N_{\alpha\nu, \iota}^{0,F} + \iota Q_{\alpha\nu}^0/2\pi$ , where  $Q_{\alpha\nu}^0/2$  is the scattering-less phase shift on the right-hand side of Eq. (7). Furthermore,  $N_{\alpha\nu, \iota}^F$  refers to the  $\alpha\nu \neq c0, s1$  branches and is the number of  $\alpha\nu$  pseudofermions of limiting bare momentum  $q = \iota q_{\alpha\nu}^0$  such that  $\iota = \pm 1$  created by the elementary processes (B). The number of  $\alpha\nu$  pseudofermions created away from the limiting bare-momentum values by the processes (A) is called  $N_{\alpha\nu}^{NF}$ .

A ground-state - excited-energy-eigenstate transition generated by elementary processes (A) and (B) leads to the energy and momentum spectrum  $l\Delta E$  and  $l\Delta P$  given in Eqs (28) and (29) of Ref. [2], respectively, where  $l = +1$  or  $l = -1$  depending on the specific spectral function (2) under consideration. Each of such excited states is associated with a well defined point  $(l\Delta E, l\Delta P)$  in the  $(k, \omega)$ -plane. A key property of the PDT is that the set or tower of excited states generated by the elementary processes (C) from each excited energy eigenstate generated by the processes (A) and (B) have the same values for the two charge parameters  $2\Delta_{c0}^{\pm 1}$  and two spin parameters  $2\Delta_{s1}^{\pm 1}$  of Eq. (1) as the latter state. The transitions to that tower of excited states generates the spectral weight in the vicinity of the corresponding point  $(l\Delta E, l\Delta P)$ . Thus, that weight is associated with the same value of the following functional, which plays a major role in the spectral properties,

$$\begin{aligned} \zeta_0 &= 2\Delta_{c0}^{+1} + 2\Delta_{c0}^{-1} + 2\Delta_{s1}^{+1} + 2\Delta_{s1}^{-1}, \\ 2\Delta_{\alpha\nu}^{\iota} &= \left( \iota \Delta N_{\alpha\nu, \iota}^F + \frac{Q_{\alpha\nu}^{\Phi}(\iota q_{F\alpha\nu}^0)}{2\pi} \right)^2, \end{aligned} \quad (10)$$

where  $\alpha\nu = c0, s1$  and  $\iota = \pm 1$ . Note that  $\zeta_0$  equals the sum of the four parameters of Eq. (1), which can be expressed in terms of the overall scattering phase shift of Eq. (4), as given in the second expression of Eq. (10). Such parameters are functionals of the pseudofermion occupancy configurations which describe the excited states generated by the elementary processes (A) and (B).

The corresponding functional expressions are given in Eqs. (12) and (40) of Ref. [2]. Thus, for each excited state generated from the initial ground state by the processes (A) and (B) there is a subspace spanned by the set of excited states generated by the processes (C) from the former excited state. Given the linear  $\alpha\nu = c0, s1$  pseudofermion energy dispersion near the *Fermi points*, the processes (C) lead to small momentum and

energy values such that,

$$k' = \sum_{\alpha\nu=c0, s1} \sum_{\iota=\pm 1} \iota \frac{2\pi}{L} m_{\alpha\nu, \iota}; \quad \omega' = \sum_{\alpha\nu=c0, s1} \sum_{\iota=\pm 1} \frac{2\pi}{L} v_{\alpha\nu} m_{\alpha\nu, \iota}. \quad (11)$$

Here  $m_{\alpha\nu, \iota}$  is the number of elementary  $\alpha\nu$  pseudofermion particle-hole processes of momentum  $\iota[2\pi/L]$ . Thus, the elementary processes (C) generate a set of excited energy eigenstates with energy  $l\Delta E$  and momentum  $l\Delta P$  given by those of the initial excited state state generated from the ground state by the processes (A) and (B), plus the small energy  $\omega'$  and momentum  $k'$  provided in Eq. (11).

Within the PDT the general  $\mathcal{N}$ -electron spectral functions (2) factorize in terms of  $\alpha\nu$  pseudofermion spectral functions. The probability amplitude  $A_{\alpha\nu}^{(0,0)}$  appears in the expressions of the latter functions for  $\alpha\nu = c0, s1$ . It is associated with the canonical-momentum densely packed configurations generated by the elementary processes (A) and (B) after the matrix elements between the ground state and the excited states generated by these processes are computed. Such a probability amplitude corresponds to the  $\alpha\nu = c0, s1$  pseudofermion spectral-function lowest-peak weight given in Eq. (48) of Ref. [2]. It has the following approximate behaviour,

$$A_{\alpha\nu}^{(0,0)} \approx \prod_{\iota=\pm 1} A_{\alpha\nu, \iota}^{(0,0)} \left[ 1 + \mathcal{O}\left(\frac{1}{N_a}\right) \right],$$

$$A_{\alpha\nu, \iota}^{(0,0)} = \frac{f_{\alpha\nu, \iota}}{\left(N_a S_{\alpha\nu}^0\right)^{-1/2+2\Delta_{\alpha\nu}^{\iota}}}; \quad \alpha\nu = c0, s1; \quad \iota = \pm 1. \quad (12)$$

Here  $2\Delta_{\alpha\nu}^{\iota}$  is the functional given in Eq. (1), and  $f_{\alpha\nu, \iota}$  reads,

$$f_{\alpha\nu, \iota} = \sqrt{f\left(Q_{\alpha\nu}(\iota q_{F\alpha\nu}^0) + \text{sgn}(\iota)\pi\right)}; \quad f_{\alpha\nu} = \prod_{\iota=\pm 1} f_{\alpha\nu, \iota}; \quad \alpha\nu = c0, s1. \quad (13)$$

In this expression,  $k$  stands for the excited-state momentum relative to the initial ground state,  $f(Q) = f(-Q)$  is the function defined in Ref. [17], which occurs on the right-hand side of Eq. (24) of that reference, and  $f_{\alpha\nu}$  appears in spectral-function expressions introduced below. Moreover,  $S_{\alpha\nu}^0$  is a  $n, m$ , and  $U/t$  dependent constant such that  $S_{c0}^0 S_{s1}^0 \rightarrow 1$  both for  $U/t \rightarrow 0$  and for  $U/t \rightarrow \infty$  and  $m \rightarrow 0$ . (From Ref. [17] we learn that  $S_{c0}^0 \rightarrow \sin(\pi n)$  for  $U/t \rightarrow \infty$  and  $m \rightarrow 0$ , and thus  $S_{s1}^0 \rightarrow 1/\sin(\pi n)$  in such a limit.) It is useful to introduce the following quantity,

$$D_0 = \prod_{\alpha\nu=c0, s1} \frac{S_{\alpha\nu}^0 f_{\alpha\nu}}{(S_{\alpha\nu}^0)^{[2\Delta_{\alpha\nu}^{+1}+2\Delta_{\alpha\nu}^{-1}]}}. \quad (14)$$

Another important piece of the  $\alpha\nu = c0, s1$  pseudofermion spectral functions is the relative weight  $a_{\alpha\nu, \iota}(m_{\alpha\nu, \iota})$  generated by the elementary processes (C) in the vicinity of the right ( $\iota = +1$ ) and left ( $\iota = -1$ ) *Fermi* points. When  $2\Delta_{\alpha\nu}^{\iota} > 0$  the weight  $a_{\alpha\nu, \iota}(m_{\alpha\nu, \iota})$  and its asymptotic expression are given in Eqs. (52) and (55) of Ref. [2], respectively. The point is that when the excited states generated by the processes (A) and (B) are such that  $2\Delta_{\alpha\nu}^{\iota} = 0$  the relative weight  $a_{\alpha\nu, \iota}(m_{\alpha\nu, \iota})$  reads instead,

$$a_{\alpha\nu, \iota}(m_{\alpha\nu, \iota}) = \delta_{m_{\alpha\nu, \iota}, 0}; \quad 2\Delta_{\alpha\nu}^{\iota} = 0; \quad \alpha\nu = c0, s1; \quad \iota = \pm 1. \quad (15)$$

Since for densities in the range  $0 < n < 1$  and  $0 < m < n$  the two charge parameters  $2\Delta_{c0}^{\pm 1}$  and two spin parameters  $2\Delta_{s1}^{\pm 1}$  are finite for all excited states, this case was not considered in the studies of Ref. [2].

As further discussed below, the general  $\mathcal{N}$ -electron spectral function given in Eq. (2) can be expressed in terms of the charge  $c0$  and spin  $s1$  spectral functions provided in Eq. (56) of Ref. [2]. Here we express the latter functions as follows,

$$B_{Q_{\alpha\nu}}^{l,i}(k', \omega') = \frac{N_a}{2\pi} \int_{-\infty}^{+\infty} dk'' \int_{-\infty}^{+\infty} d\omega'' B_{Q_{\alpha\nu}}^{l,\iota,i}(k' - k'', \omega' - \omega'') \times B_{Q_{\alpha\nu}}^{l,-\iota,i}(k'', \omega''); \quad \alpha\nu = c0, s1; \quad \iota = \pm 1. \quad (16)$$

The studies of Ref. [2] refer to the case where the two charge parameters  $2\Delta_{c0}^{\pm 1}$  and two spin parameters  $2\Delta_{s1}^{\pm 1}$  are finite. In that case the four relative weights  $a_{\alpha\nu,\iota}(m_{\alpha\nu,\iota})$  such that  $\alpha\nu = c0, s1$  and  $\iota = \pm 1$  and their asymptotic expressions are of the form provided in Eqs. (52) and (55) of Ref. [2], respectively, and thus the functions  $B_{Q_{\alpha\nu}}^{l,\iota,i}(k', \omega')$  on the right-hand side of Eq. (16) are given by [2],

$$B_{Q_{\alpha\nu}}^{l,\iota,i}(k', \omega') = \frac{A_{\alpha\nu,\iota}^{(0,0)}}{v_{\alpha\nu}} a_{\alpha\nu,\iota} \left( \frac{l\omega'}{2\pi v_{\alpha\nu}/N_a} \right) \delta\left(k' - \frac{\iota\omega'}{v_{\alpha\nu}}\right) \approx \frac{f_{\alpha\nu,\iota}}{v_{\alpha\nu}} \frac{\Theta(l\omega')}{\sqrt{N_a S_{\alpha\nu}^0}} \left( \frac{l\omega'}{2\pi v_{\alpha\nu} S_{\alpha\nu}^0} \right)^{2\Delta_{\alpha\nu}^{\iota}-1} \delta\left(k' - \frac{\iota\omega'}{v_{\alpha\nu}}\right), \quad (17)$$

where  $\alpha\nu = c0, s1$  and  $\iota = \pm 1$ . The second expression corresponds to the asymptotic behaviour valid for small finite values of  $l\omega'$ .

However, when  $2\Delta_{\alpha\nu}^{\iota} = 0$  the corresponding relative weight  $a_{\alpha\nu,\iota}(m_{\alpha\nu,\iota})$  is of the form provided in Eq. (15) and thus the spectral function  $B_{Q_{\alpha\nu}}^{l,\iota,i}(k', \omega')$  instead of being given by Eq. (17) reads,

$$B_{Q_{\alpha\nu}}^{l,\iota,i}(k', \omega') = \frac{2\pi}{N_a} A_{\alpha\nu,\iota}^{(0,0)} \delta(k') \delta(\omega') \approx 2\pi f_{\alpha\nu,\iota} \sqrt{\frac{S_{\alpha\nu}^0}{N_a}} \delta(k') \delta(\omega'); \quad \alpha\nu = c0, s1; \quad \iota = \pm 1. \quad (18)$$

In order to reach the correct spectral-function expressions for all electronic densities of the metallic phase and for  $m \rightarrow 0$ , several cases must be considered. The first corresponds to excited states such that the two charge parameters  $2\Delta_{c0}^{\pm 1}$  and two spin parameters  $2\Delta_{s1}^{\pm 1}$  are finite. The two functions on the right-hand side of Eq. (16) are of the form given in Eq. (17) and thus we find,

$$B_{Q_{\alpha\nu}}^{l,i}(k', \omega') = \frac{L}{4\pi v_{\alpha\nu}} A_{\alpha\nu}^{(0,0)} \prod_{\iota=\pm 1} a_{\alpha\nu,\iota} \left( \frac{l[\omega' + \iota v_{\alpha\nu} k']}{4\pi v_{\alpha\nu}/N_a} \right) \approx \frac{f_{\alpha\nu}}{4\pi v_{\alpha\nu} S_{\alpha\nu}^0} \prod_{\iota=\pm 1} \frac{\Theta(l[\omega' + \iota v_{\alpha\nu} k'])}{\Gamma(2\Delta_{\alpha\nu}^{\iota})} \left( \frac{l[\omega' + \iota v_{\alpha\nu} k']}{4\pi v_{\alpha\nu} S_{\alpha\nu}^0} \right)^{2\Delta_{\alpha\nu}^{\iota}-1}, \quad (19)$$

where  $\alpha\nu = c0, s1$ . The second expression corresponds to the asymptotic behaviour valid for small finite values of  $l[\omega' + \iota v_{\alpha\nu} k']$ . This function is that already given in Eq.

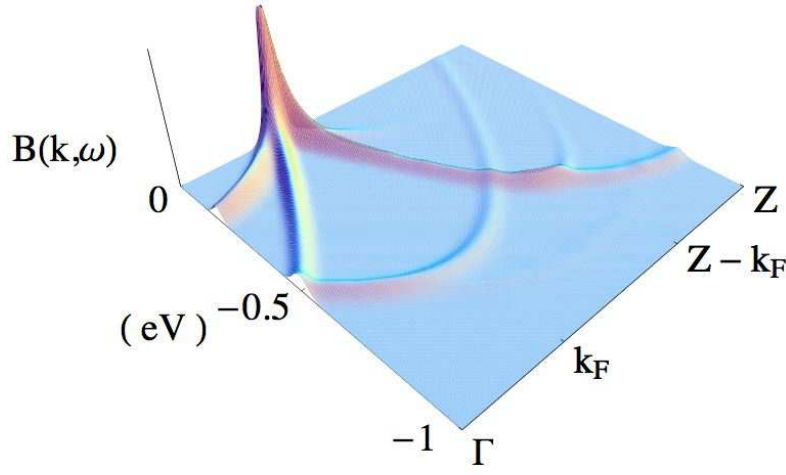


**Figure 1.** Full theoretical line shape of the one-electron removal spectral-weight distribution found in Ref. [4] to fit the corresponding spectral features of TTF-TCNQ. The spectrum shown here is rotated relative to that shown in Fig. 2 of that reference. It includes both the TTF related spectral features for  $n = 1.41$ ;  $t = 0.35$  eV;  $U/t = 5.61$  and those of TCNQ for  $n = 0.59$ ;  $t = 0.40$  eV;  $U/t = 4.90$ , respectively.

(56) of Ref. [2]. (See the note [25] concerning a discrepancy of a factor 2 between the function given here and that provided in Eq. (56) of Ref. [2] and how a misprint in the latter equation becomes an error, by propagating to other expressions of Refs. [2, 7].)

The second case occurs when the excited states are such that for the functions on the right-hand side of Eq. (16) one has that  $2\Delta_{\alpha\nu}^{\iota} > 0$  and  $2\Delta_{\alpha\nu}^{-\iota} = 0$ . Then one must use in that equation the expression (17) for the function  $B_{Q_{\alpha\nu}}^{l,\iota,i}(k', \omega')$  and that given in Eq. (18) for the function  $B_{Q_{\alpha\nu}}^{l,-\iota,i}(k', \omega')$ . This leads to the following expression for the function on the left-hand side of Eq. (16),

$$\begin{aligned} B_{Q_{\alpha\nu}}^{l,i}(k', \omega') &= \frac{A_{\alpha\nu}^{(0,0)}}{v_{\alpha\nu}} a_{\alpha\nu,\iota} \left( \frac{l\omega'}{2\pi v_{\alpha\nu}/N_a} \right) \delta\left(k' - \frac{\iota\omega'}{v_{\alpha\nu}}\right) \\ &\approx \frac{f_{\alpha\nu}}{v_{\alpha\nu} \Gamma(2\Delta_{\alpha\nu}^{\iota})} \Theta(l\omega') \left( \frac{l\omega'}{2\pi v_{\alpha\nu} S_{\alpha\nu}^0} \right)^{2\Delta_{\alpha\nu}^{\iota}-1} \delta\left(k' - \frac{\iota\omega'}{v_{\alpha\nu}}\right), \end{aligned} \quad (20)$$

where  $\alpha\nu = c0, s1$  and  $\iota = \pm 1$ .

Finally, the third case refers to excited states such that for the functions on the right-hand side of Eq. (16) one has that  $2\Delta_{\alpha\nu}^{\iota} = 2\Delta_{\alpha\nu}^{-\iota} = 0$ . In this case one must use in that equation the expression (18) for both the functions  $B_{Q_{\alpha\nu}}^{l,\iota,i}(k', \omega')$  and  $B_{Q_{\alpha\nu}}^{l,-\iota,i}(k', \omega')$ . One then reaches the following expression for the function on the left-hand side of Eq. (16),

$$B_{Q_{\alpha\nu}}^{l,i}(k', \omega') = \frac{2\pi}{N_a} A_{\alpha\nu}^{(0,0)} \delta(k') \delta(\omega')$$

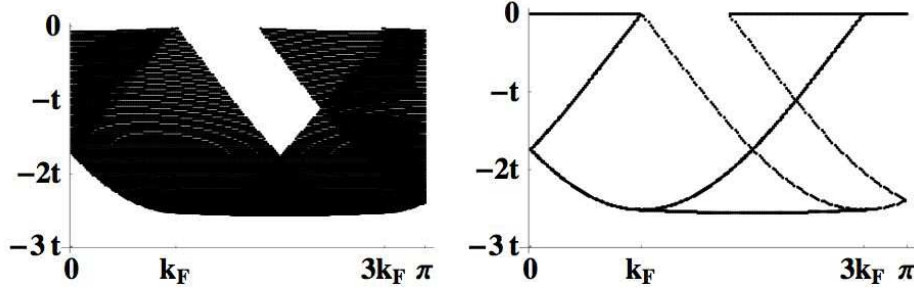


**Figure 2.** The region of the  $(k, \omega)$  plane with a finite one-electron removal spectral weight obtained by running over all the momentum values of the  $c0$  and  $s1$  momentum distribution deviations of Eqs. (32) and (33) for  $U/t = 100$ ,  $n = 0.59$ , and  $m \rightarrow 0$ . The corresponding branch and border lines are also plotted.

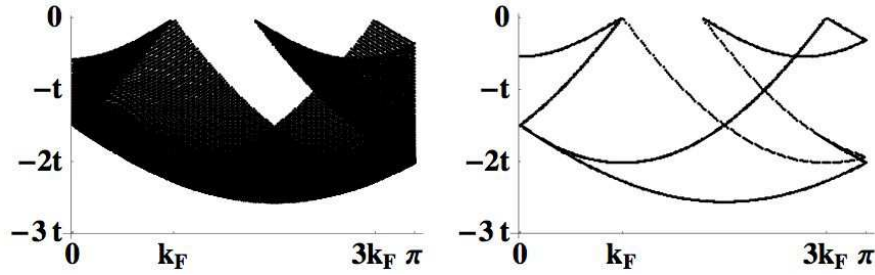


**Figure 3.** The same region of the  $(k, \omega)$  plane and branch and border lines as in Fig. 2 for  $U/t = 4.9$ ,  $n = 0.59$ , and  $m \rightarrow 0$ .

$$\approx 2\pi f_{\alpha\nu} S_{\alpha\nu}^0 \delta(k') \delta(\omega'); \quad \alpha\nu = c0, s1. \quad (21)$$

The general PDT expression for the  $\mathcal{N}$ -electron spectral function given in Eq. (2) reads [2],

$$B_{\mathcal{N}}^l(k, \omega) = \sum_{i=0}^{\infty} c_i^l \sum_{\{\Delta N_{\alpha\nu}\}, \{L_{\alpha, -1/2}\}} \left[ \sum_{\{N_{\alpha\nu}^{phNF}\}, \{\Delta N_{\alpha\nu}^F, i\}, \{N_{\alpha\nu}^F\}} B^{l,i}(k, \omega) \right], \quad (22)$$

where  $c_0^l = 1$ ,  $l = \pm 1$ , and for densities  $0 < n < 1$  the summation over the numbers  $N_{\alpha\nu}^{phNF}$  is limited to finite values. On the right-hand side of Eq. (22),  $c_i^l$  is the constant of the operator expressions given in Eqs. (32)-(34) of Ref. [3] such that  $c_i^l \rightarrow 0$  as  $U/t \rightarrow \infty$  for  $i > 0$  and the function  $B^{l,i}(k, \omega)$  is defined in Eq. (44) of Ref. [2]. The latter function is fully defined by the related function  $\check{B}^{l,i}(\Delta\omega, v)$ . However, the second expression for  $\check{B}^{l,i}(\Delta\omega, v)$  given in Eq. (45) of Ref. [2] is only valid for  $v_{c0} > v_{s1}$ . For finite values of  $U/t$  this excludes electronic densities in the vicinity of 1.

Generalization of  $\check{B}^{l,i}(\Delta\omega, v)$  for the whole range of electronic densities of the metallic phase, including densities such that the spin and charge velocities obey the inequality  $v_{s1} > v_{c0}$ , leads to the following expression,

$$\begin{aligned} \check{B}^{l,i}(\Delta\omega, v) &= \frac{\text{sgn}(v)}{2\pi} \int_0^{\Delta\omega} d\omega' \int_{-\text{sgn}(v)\Delta\omega/v_{\alpha\nu}}^{+\text{sgn}(v)\Delta\omega/v_{\alpha\nu}} dk' \\ &\times B_{Q_{\alpha\nu}}^{l,i}(\Delta\omega/v - k', \Delta\omega - \omega') B_{Q_{\alpha\nu}}^{l,i}(k', \omega'). \end{aligned} \quad (23)$$

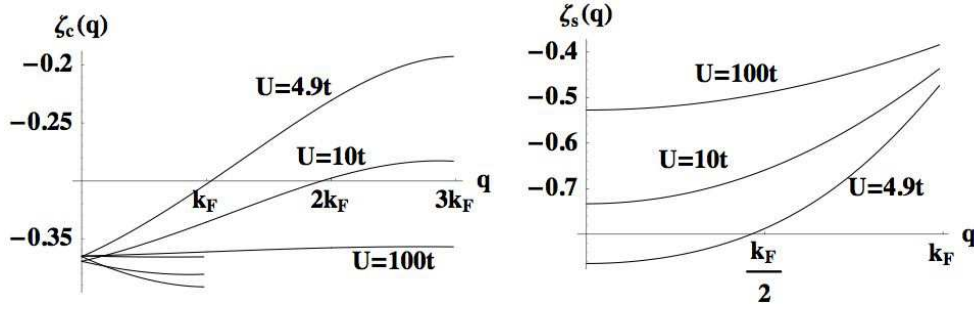


**Figure 4.** The value of the  $c0$  and  $s1$  branch lines exponents of the one-electron removal weight distribution as a function of momentum for  $n = 0.59$ ,  $m \rightarrow 0$ , and several magnitudes of  $U/t$ . The exponents of index  $c$  and  $s$  refer to the  $c0$  and  $s1$  branch lines, respectively.

In this equation, in those provided in Appendix A, and in the whole our analysis until subsection 3.2 we use a notation for the charge branch  $c0$  and spin branch  $s1$  such that  $\alpha\nu = c0, s1$  when the branch index  $\bar{\alpha}\bar{\nu}$  defined by Eq. (9) reads  $\bar{c}\bar{0} = s1, c0$ , respectively. Moreover, in equation (23)  $l = +1$  or  $l = -1$  according to the  $\mathcal{N}$ -electron spectral function (2) under consideration,  $\Delta\omega = (\omega - l\Delta E)$ ,  $\Delta k = (k - l\Delta P)$ , and  $l\Delta E$  and  $l\Delta P$  correspond to the general energy and momentum spectra given in Eqs. (28) and (29) of Ref. [2], respectively, which is generated by the elementary processes (A) and (B),  $i = 0, 1, 2, \dots$ , and for  $i > 0$  the index  $i = 1, 2, \dots$  is a positive integer number which increases for increasing values of the number of extra pairs of creation and annihilation rotated-electron operators in the expressions of the pseudofermion operators associated with the function  $\check{B}^{l,i}(\Delta\omega, v)$  relative to that of the pseudofermion operators of the  $i = 0$  function  $\check{B}^{l,0}(\Delta\omega, v)$  [2]. Expression (23) is valid for the whole  $(k, \omega)$ -plane, except for  $k$  and  $\omega$  values such that  $\omega \approx \nu v_{\alpha\nu}(k - lk_0) + l\omega_0$ , where  $\alpha\nu = c0, s1$ ,  $\nu = \pm 1$ ,  $\omega_0$  and  $k_0$  are provided in Eqs. (32) and (34) of Ref. [2].

The velocity  $v$  appearing in the argument of the function (23) plays an important role in our study and is given by,

$$v = \frac{\Delta\omega}{\Delta k} = \frac{(\omega - l\Delta E)}{(k - l\Delta P)}; \quad \text{sgn}(v) 1 = \text{sgn}(\Delta k) l; \quad |v| > v_{\bar{\alpha}\bar{\nu}}. \quad (24)$$

The inequality  $|v| > v_{\bar{\alpha}\bar{\nu}}$  follows from the structure of the spectrum of Eq. (31) of Ref. [2].

When at least one of the two parameters  $2\Delta_{\alpha\nu}^{\pm 1}$  and two parameters  $2\Delta_{\bar{\alpha}\bar{\nu}}^{\pm 1}$  is finite, use of the general expression (23) for the function  $\check{B}^{l,i}(\Delta\omega, v)$  for small finite values of  $l\Delta\omega = l(\omega - l\Delta E)$  with  $B_{Q_{\alpha\nu}}^{l,i}(k', \omega')$  and  $B_{Q_{\bar{\alpha}\bar{\nu}}}^{l,i}(k', \omega')$  equaling the suitable expressions provided in Eqs. (19), (20), and (21) leads to the following asymptotic behaviour for that convolution function,

$$\check{B}^{l,i}(\Delta\omega, v) \approx \frac{F_0(1/v)}{4\pi\sqrt{v_{c0}v_{s1}}} \Theta(l\Delta\omega) \left( \frac{l\Delta\omega}{4\pi\sqrt{v_{c0}v_{s1}}} \right)^{-2+\zeta_0}. \quad (25)$$

Here  $i = 0, 1, 2, \dots$ ,  $l = \pm 1$ , and  $\zeta_0$  is the functional provided in Eq. (10) and the pre-factor function  $F_0(z)$  is given in Appendix A. In turn, if all four above parameters

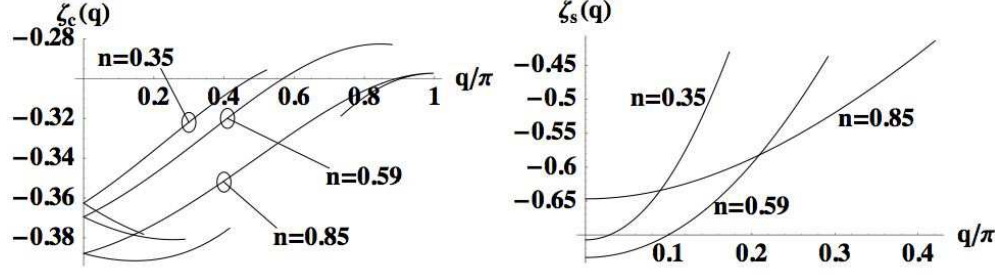


**Figure 5.** The same exponents as in Fig. 4 as a function of momentum for  $U/t = 10$ ,  $m \rightarrow 0$ , and several values of  $n$ .

vanish we find by use of expression (23) with  $B_{Q_{\alpha\nu}}^{l,i}(k', \omega')$  and  $B_{Q_{\bar{\alpha}\bar{\nu}}}^{l,i}(k', \omega')$  of the form given in Eq. (21) that,

$$\check{B}^{l,i}(\Delta\omega, v) = \bar{B}^{l,i}(\Delta\omega, \Delta k) = 2\pi D_0 \delta(\Delta\omega)\delta(\Delta k), \quad (26)$$

where  $D_0$  is defined in Eq. (14), in agreement with the first expression of Eq. (59) of Ref. [2] for  $\zeta_0 = 0$ .

Depending on the values of the two parameters  $2\Delta_{\alpha\nu}^{\pm 1}$  and two parameters  $2\Delta_{\bar{\alpha}\bar{\nu}}^{\pm 1}$ , we consider in Appendix A seven cases where by use of Eqs. (19), (20), (21), (23), and (25) a set of alternative expressions for the pre-factor function  $F_0(z)$  on the right-hand side of the latter equation can be derived and are given in that Appendix. Expressions (A.1)-(A.7) of the same Appendix provide a generalization of the pre-factor function  $F_0(z)$  given in Eq. (62) of Ref. [2]. The latter function corresponds to the general function (A.1) of Appendix A for  $\alpha\nu = c0$  [25]. The recent studies of Ref. [4] on the finite-energy spectral features of the organic compound TTF-TCNQ use the functions (A.1)-(A.7) of that Appendix derived in this paper.

Importantly, general spectral-function expressions for all electronic densities of the metallic phase are obtained by replacing the spin velocity  $v_{s1}$  by  $v_{\bar{\alpha}\bar{\nu}}$  in the limits of the variable  $z$  integrations of expressions (66) and (B.14) of Ref. [2] and both in the limits of the variable  $z$  integrations and arguments of the theta-functions of expressions (71), (B.17), and (B.18) of the same reference. After such replacements, Eqs. (66), (68), (70), and (71) of Ref. [2] with the pre-factor function  $F_0(z)$  given in Eqs. (A.1)-(A.7) of Appendix A provide general spectral-function expressions for all electronic densities of the metallic phase and spin densities in the range  $0 \leq m < n$ . However, note that while the branch index  $\bar{\alpha}\bar{\nu}$  is that defined by Eq. (9), the branch indices  $\alpha\nu$  and  $\alpha'\nu'$  of Eqs. (66) and (B.14) of Ref. [2] correspond to the two created quantum objects and in contrast to the branch index  $\alpha\nu$  of Eqs. (23)-(26) and (A.1)-(A.7) of Appendix A there are no restrictions imposing that such branch indices are different or equal to the branch index  $\bar{\alpha}\bar{\nu}$ , the same applying to the branch index  $\alpha\nu$  of Eqs. (70), (71), (B.17), and (B.18) of that reference.

It is straightforward to show that the double Fourier transform of the function (18) equals that of the function (17) as  $2\Delta_{\alpha\nu}^l \rightarrow 0$ . It follows that the asymptotic

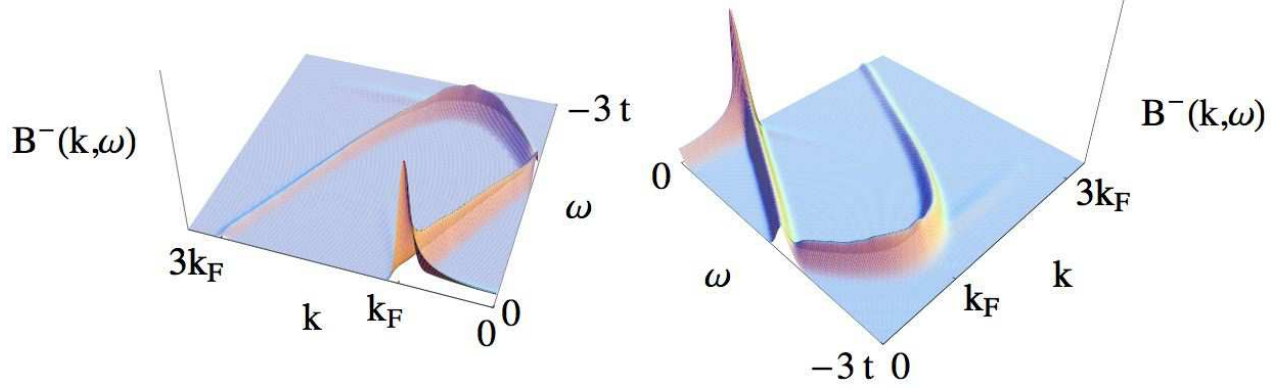


**Figure 6.** Full PDT one-electron removal spectral-weight distribution associated with the  $c_0$  and  $s_1$  momentum deviations of Eqs. (32) and (33) and corresponding functionals given in Eqs. (34) and (35) for  $U/t = 100$ ,  $n = 0.59$ , and  $m \rightarrow 0$ .

expression of the correlation function given in Eq. (32) of Ref. [7] is of the general form provided in Eq. (52) of that reference independently on whether all four parameters  $2\Delta_{\alpha\nu}^{\iota}$  where  $\alpha\nu = c_0, s_1$  and  $\iota = \pm 1$  are finite or some of these parameters vanish. Thus, the different expressions (A.1)-(A.7) of Appendix A for the pre-factor  $F_0(z)$  of the convolution function (25) are not associated with different pre-factors for the corresponding correlation-function expression (52) of Ref. [7]. The pre-factor of the latter function is always of the form given in Eq. (50) of that reference [25].

### 3.2. Explicit spectral-function expressions in the vicinity of the border lines

The singular features of the  $\mathcal{N}$ -electron spectral functions (2) are of power law type. The power-law branch-line singular features of general form given in Eqs. (68) and (71) of Ref. [2] are controlled by non-classic interaction, density, and momentum dependent exponents. The spectral feature of general form given in Eqs. (66) of that reference can also include power-law singular features called border lines. However, the studies of Ref. [2] did not provide an explicit general expression for the  $k$  and  $\omega$  dependence in the vicinity the border lines. Here we provide such an expression and find that for the border lines the power-law exponent has an universal value given by  $-1/2$ .

The shape  $\omega = \omega_{BL}(k)$  of a border line is defined by the following parametric equations [2],

$$\begin{aligned} \omega_{BL}(k) &= l[\omega_0 + c'_1 \epsilon_{\alpha'\nu'}(q') + c''_1 \epsilon_{\alpha''\nu''}(q'')] \delta_{v_{\alpha'\nu'}(q'), v_{\alpha''\nu''}(q'')}, \\ k &= lk_{\alpha'\nu', \alpha''\nu''}(q', q'') \delta_{v_{\alpha'\nu'}(q'), v_{\alpha''\nu''}(q'')}. \end{aligned} \quad (27)$$

Here  $q'$  and  $q''$  are the bare-momentum values of the  $\alpha'\nu'$  and  $\alpha''\nu''$ , respectively,

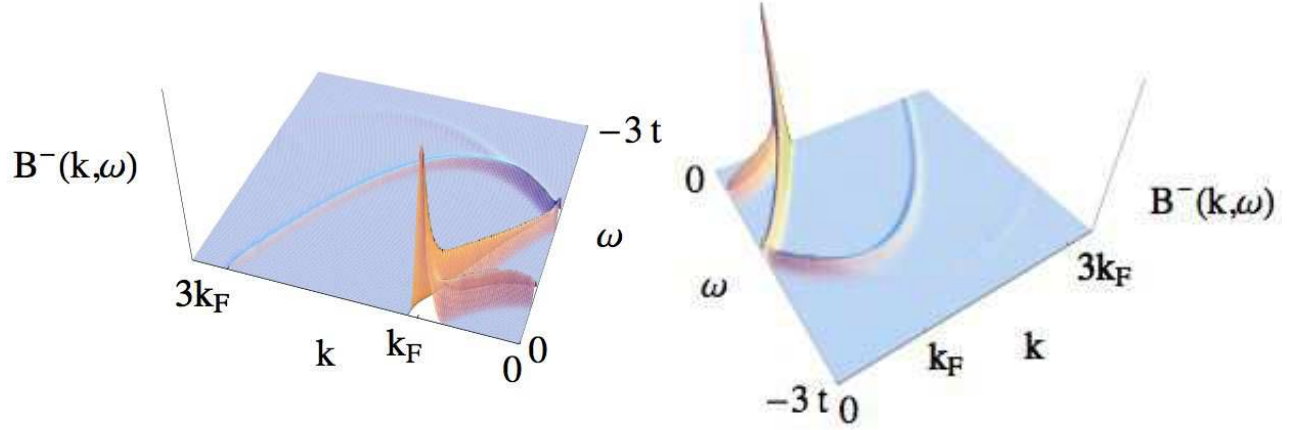


**Figure 7.** The same PDT one-electron removal spectral-weight distribution as in Fig. 6 for the values  $U/t = 4.9$ ,  $n = 0.59$ , and  $m \rightarrow 0$  suitable to the TCNQ related spectral features.

pseudofermion or pseudofermion-hole scattering centers created by the processes (A),  $c'_1, c''_1 = +1$  for pseudofermion creation and  $c'_1, c''_1 = -1$  for pseudofermion-hole creation,  $\omega_0$  is the finite-energy parameter given in Eq. (32) of Ref. [2], and  $k_{\alpha'\nu'}, k_{\alpha''\nu''}(q', q'')$  is the momentum spectrum provided in Eqs. (64) and (65) of that reference. As for Eqs. (66) and (B.14) of Ref. [2] and in contrast to the branch index  $\alpha\nu$  of Eqs. (23)-(A.7), there are no restrictions imposing that the branch indices  $\alpha'\nu'$  and  $\alpha''\nu''$  of the two created scattering centers are different or equal to the branch index  $\bar{\alpha}\bar{\nu}$  defined by Eq. (9).

By use of methods similar to those used in Ref. [2] for other weight distributions, we find that the spectral function has the following singular behaviour in the vicinity and just below ( $l = +1$ ) or above ( $l = -1$ ) the border line,

$$\begin{aligned}
 B_{\mathcal{N}}^l(k, \omega) &\approx \frac{2 \Theta(\Omega - l[\omega_{BL}(k) - \omega])}{\pi C_c C_s \zeta_0(q', q'') \sqrt{|a_{\alpha'\nu'}(q')| + |a_{\alpha''\nu''}(q'')|}} \\
 &\times \left[ \int_{-1/v_{\bar{\alpha}\bar{\nu}}}^{+1/v_{\bar{\alpha}\bar{\nu}}} dz F_0(z) \right] \\
 &\times \left( \frac{\Omega}{4\pi \sqrt{v_{c0} v_{s1}}} \right)^{\zeta_0(q', q'')} \left( \frac{2l[\omega_{BL}(k) - \omega]}{v_{c0} v_{s1}} \right)^{-\frac{1}{2}}, \quad (28)
 \end{aligned}$$

where  $a_{\alpha\nu}(q) = \partial v_{\alpha\nu}(q)/\partial q$ . In turn, just above ( $l = +1$ ) or below ( $l = -1$ ) the line the weight distribution reads,

$$B_{\mathcal{N}}^l(k, \omega) \approx \frac{2 \Theta(\Omega - l[\omega - \omega_{BL}(k)])}{\pi C_c C_s \zeta_0(q', q'') \sqrt{|a_{\alpha'\nu'}(q')| + |a_{\alpha''\nu''}(q'')|}}$$

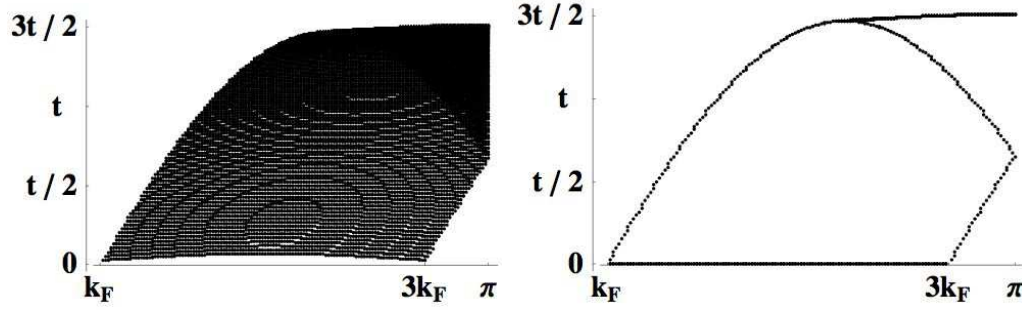


**Figure 8.** The region of the  $(k, \omega)$  plane with a finite one-electron addition spectral weight obtained by running over all the momentum values of the  $c0$  and  $s1$  momentum distribution deviations of Eqs. (32) and (33) for  $U/t = 100$ ,  $n = 0.59$ , and  $m \rightarrow 0$ . The corresponding branch and border lines are also shown.

$$\begin{aligned}
 & \times \left\{ \Theta \left( v_{\bar{\alpha}\bar{\nu}} \left[ 1 - \frac{l[\omega - \omega_{BL}(k)]}{\Omega} \right] - |v_{\alpha'\nu'}(q')| \right) \int_{\frac{-1}{v_{\bar{\alpha}\bar{\nu}}}^{\frac{1}{v_{\bar{\alpha}\bar{\nu}}}} dz F_0(z) \right. \\
 & + \text{sgn}(q') \theta \left( |v_{\alpha'\nu'}(q')| - v_{\bar{\alpha}\bar{\nu}} \left[ 1 - \frac{l[\omega - \omega_{BL}(k)]}{\Omega} \right] \right) \\
 & \times \left. \int_{-\frac{\text{sgn}(q')1}{v_{\bar{\alpha}\bar{\nu}}}^{\frac{1}{v_{\alpha'\nu'}(q')} \left( 1 - \frac{l[\omega - \omega_{BL}(k)]}{\Omega} \right)} dz F_0(z) \right\} \\
 & \times \left[ \left( \frac{\Omega}{4\pi\sqrt{v_{c0}v_{s1}}} \right)^{\zeta_0(q', q'')} - \left( \frac{l[\omega - \omega_{BL}(k)]}{4\pi\sqrt{v_{c0}v_{s1}} [1 - z v_{\alpha'\nu'}(q')]} \right)^{\zeta_0(q', q'')} \right] \\
 & \times \left( \frac{2l[\omega - \omega_{BL}(k)]}{v_{c0}v_{s1}} \right)^{-\frac{1}{2}}, \tag{29}
 \end{aligned}$$

where  $\theta(x) = 0$  for  $x \leq 0$  and  $\theta(x) = 1$  for  $x > 0$ ,  $\Omega$  is the energy cut off of the elementary processes (C) defined in Ref. [2],  $\zeta_0 = \zeta_0(q', q'')$  is the functional given in Eq. (10) for the excited states which contribute to the weight distribution (66) of that reference, and  $C_c$  and  $C_s$  are defined in Eq. (68) of Ref. [3].

#### 4. APPLICATIONS OF THE PSEUDOFERMION DYNAMICAL THEORY TO THE SPECTRUM OF TTF-TCNQ

As discussed in Ref. [4], the spectral-weight distribution of TTF-TCNQ is fully determined by the occupancy configurations of the  $c$  and  $s1$  pseudofermions in the one-electron excited states. The studies of that reference reveal that for electronic density  $n = 1.41$  the electron removal spectrum calculated for  $t = 0.35$  eV and  $U = 1.96$  eV ( $U/t = 5.61$ ) yields the best agreement with the TTF related experimental dispersions. In turn, for electronic density  $n = 0.59$  an almost perfect agreement with the TCNQ related experimental dispersions is reached for the finite-energy-electron-removal spectrum calculated for  $t = 0.40$  eV and  $U = 1.96$  eV ( $U/t = 4.90$ ) [4, 18].

If one profits from the model particle-hole symmetry, one can achieve the one-electron removal spectrum at  $n = 1.41$  and a given  $U/t$  value from the one-electron

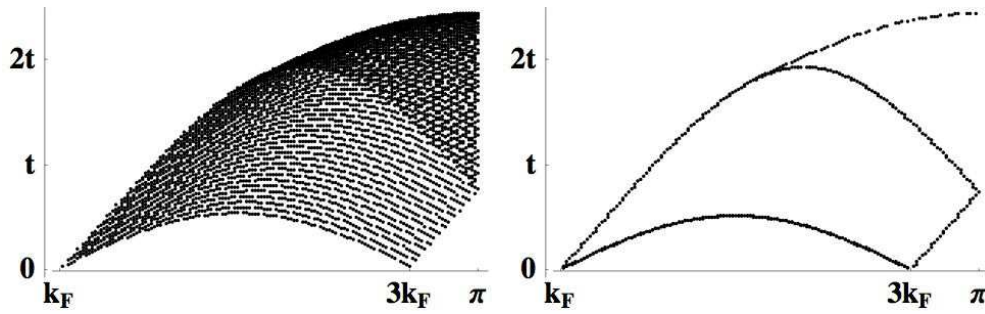


**Figure 9.** The same region of the  $(k, \omega)$  plane and branch and border lines as in Fig. 8 for  $U/t = 5.61$ ,  $n = 0.59$ , and  $m \rightarrow 0$ .

addition spectrum at  $n = 0.59$  and the same value of  $U/t$ . The full theoretical line shape of the one-electron removal spectral-weight distribution found in Ref. [4] to fit the corresponding spectral features of TTF-TCNQ is shown in Fig. 1. Note that here such a spectrum is rotated relative to that shown in Fig. 2 of that reference.

Let us consider the processes that contribute to the spectrum of Fig. 1. Each of the corresponding spectral-weight contributions to the full one-electron spectrum plotted in that figure are obtained by use of the PDT expressions provided in the previous section and Ref. [2]. In addition to the values of  $U/t$  and  $n$  specific to TTF-TCNQ, some of the spectral contributions plotted below refer to variations in these parameters. That allows us to study how the spectral features evolve under such variations. The study of the spectral-weight peaces contributing to the full spectrum plotted in Fig. 1 allows the identification of the contributions from the different expressions considered in the previous section and Ref. [2], including the border line expressions derived in this paper and provided in Eqs. (28) and (29).

The one-electron removal spectral-weight distribution of Fig. 1 has two main contributions referring to the TCNQ and TTF related spectral features, respectively. The TCNQ related spectrum is obtained by considering the one-electron removal spectral function for  $n = 0.59$ ;  $t = 0.40$  eV;  $U/t = 4.90$ . In turn, we profit from the model particle-hole symmetry to derive the TTF related photoemission spectrum for  $n = 1.41$ ;  $t = 0.35$  eV;  $U/t = 5.61$  from the corresponding one-electron addition spectrum for  $n = 0.59$ ;  $t = 0.35$  eV;  $U/t = 5.61$  and changing the energy and momentum signs.

Nearly the whole one-electron removal spectral weight corresponds to excitations described by the following deviations from the ground-state  $N_{\alpha\nu}$   $\alpha\nu$  pseudofermion numbers and  $N_{\alpha\nu}^h$   $\alpha\nu$  pseudofermion-hole numbers where  $\alpha\nu = c0, s1$ ,

$$\Delta N_{c0} = -\Delta N_{c0}^h = -1; \quad \Delta N_{s1} = -\Delta N_{s1}^h = -1, \quad (30)$$

and with the numbers  $Q_{\alpha\nu}^0/2$  appearing on the right-hand side of Eq. (7) reading,

$$Q_{c0}^0/2 = \pm\pi/2; \quad Q_{s1}^0/2 = 0. \quad (31)$$

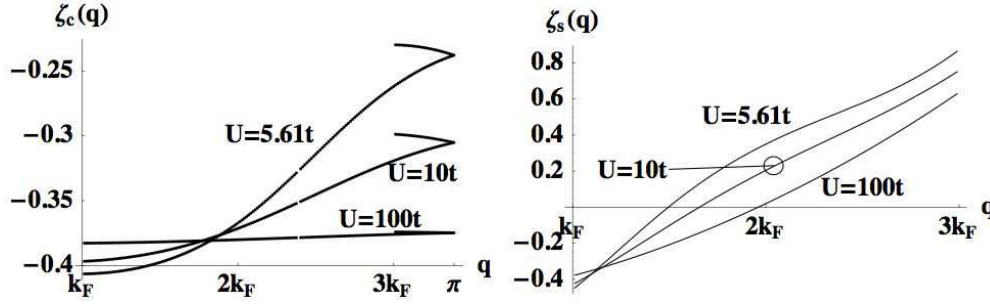


**Figure 10.** The value of the  $c_0$  and  $s_1$  branch lines exponents of the one-electron addition spectral-weight distribution as a function of momentum for  $n = 0.59$ ,  $m \rightarrow 0$ , and several magnitudes of  $U/t$ . The exponents of index  $c$  and  $s$  refer to the  $c_0$  and  $s_1$  branch lines, respectively.

If we consider bare-momentum continuum values, the general deviations read,

$$\begin{aligned} \Delta N_{c_0}(q) &= -\frac{2\pi}{L} \delta(q - q_1) - \frac{\pi}{L} \delta(q \mp 2k_F) \\ &\quad + \frac{\pi}{L} \delta(q \pm 2k_F); \quad q_1 \in [-2k_F, +2k_F] \\ \Delta N_{s_1}(q) &= -\frac{2\pi}{L} \delta(q - q'_1); \quad q'_1 \in [-k_{F\downarrow}, +k_{F\downarrow}], \end{aligned} \quad (32)$$

and thus

$$\Delta N_{s_1}(q) = -\frac{2\pi}{L} \delta(q - q'_1); \quad q'_1 \in [-k_F, +k_F] \quad (33)$$

as  $m \rightarrow 0$  for the initial ground state. Such deviations and numbers (31) are then used in the general functional  $Q_{\alpha\nu}(q_j)/2$  given in Eq. (7), whose functional  $Q_{\alpha\nu}^\Phi(q_j)/2$  is defined in Eq. (4). Such a procedure leads to,

$$\begin{aligned} Q_{c_0}(q)/2 &= \pm \pi/2 - \pi\Phi_{c_0, c_0}(q, q_1) - \pi\Phi_{c_0, c_0}(q, \mp 2k_F)/2 \\ &\quad + \pi\Phi_{c_0, c_0}(q, \pm 2k_F)/2 - \pi\Phi_{c_0, s_1}(q, q'_1), \end{aligned} \quad (34)$$

and

$$\begin{aligned} Q_{s_1}(q)/2 &= -\pi\Phi_{s_1, c_0}(q, q_1) - \pi\Phi_{s_1, c_0}(q, \mp 2k_F)/2 \\ &\quad + \pi\Phi_{s_1, c_0}(q, \pm 2k_F)/2 - \pi\Phi_{s_1, s_1}(q, q'_1), \end{aligned} \quad (35)$$

respectively.

The creation of the holes in the  $c_0$  and  $s_1$  bands whose energy dispersions are plotted in Figs. 6 and 7 of Ref. [15], respectively, corresponds for  $U/t = 100$ ,  $n = 0.59$ , and  $m \rightarrow 0$  to a finite spectral-weight distribution in the region of the  $(k, \omega)$  plane shown in Fig. 2. The lines associated with the branch lines and border lines in the finite-weight distribution are also shown. Most lines of the one-electron spectral-weight distribution plotted in Fig. 1 corresponding to power-law singularities are of the branch line type. In contrast to the border-line singularities of expressions (28) and (29), whose exponent  $-1/2$  is momentum and  $U/t$  independent, that controlling the branch-line power-law singularities is both momentum and interaction dependent. Near a branch

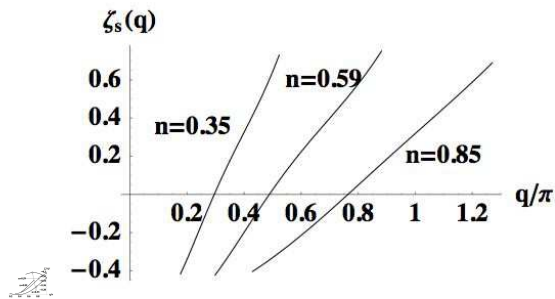


**Figure 11.** The same exponents as in Fig. 10 as a function of momentum for  $U/t = 10$ ,  $m \rightarrow 0$ , and several values of  $n$ .

line the general expression of the weight distribution is that provided in Eq. (70) of Ref. [2]. Only for momentum and interaction values where the exponent of that expression is negative is the corresponding line called a branch line. For the limit  $m \rightarrow 0$  considered here the pre-factor function  $F_0(z)$  appearing in such a branch-line expression is that given in Eqs. (A.1)-(A.7) of Appendix A. The expressions provided in the latter equations are a generalization of the pre-factor function  $F_0(z)$  of Eq. (62) of Ref. [2]. The latter applies solely when  $0 < n < 1$  and  $0 < m < n$ .

In figure 3 the same finite one-electron removal spectral-weight region and corresponding lines are shown for the  $U/t = 4.9$ ,  $n = 0.59$ , and  $m \rightarrow 0$  values suitable to the TCNQ related spectral features. Consistently with the  $U/t$  dependence of the energy bandwidth of the  $s1$  pseudofermion dispersion plotted in Fig. 7 of Ref. [15], note that the border line connecting the minimum energy points of the two  $c0$ -branch lines has  $v_{c0}(q) = v_{s1}(q') \approx 0$ . Upon decreasing the  $U/t$  value to that  $U/t = 4.9$  suitable to the TCNQ related spectral features of Fig. 1, such a border line acquires a curvature. The curvature achieved at  $U/t = 4.9$  is that behind the agreement found in Ref. [4] between the PDT predictions and the photoemission spectral features of TTF-TCNQ. That agreement is not obtained for larger or smaller values of  $U/t$ .

The (negative-exponent)  $c0$  branch line of the weight distributions of Figs. 2 and 3 runs between the excitation momenta  $-k_F$  and  $3k_F$  and the  $s1$  branch line from  $-k_F$  to  $k_F$ . The corresponding power-law momentum dependent exponents are plotted in Fig. 4 for  $n = 0.59$ ,  $m \rightarrow 0$ , and several values of  $U/t$ . The  $c0$  branch line segment between  $-k_F$  and 0 is folded in the positive momentum region. While the negative  $c0$  branch line exponent is smaller for  $U/t$  large, the negative  $s1$  branch line exponent is smaller for smaller values of  $U/t$ . In order to illustrate how systematic variations in the parameters lead to the evolution of the spectral features, the same exponents as in Fig. 4 are plotted in Fig. 5 as a function of momentum for  $U/t = 10$ ,  $m \rightarrow 0$ , and several values of  $n$ .

The use in the general PDT expressions provided in this paper and in Ref. [2] of the specific  $c0$  and  $s1$  momentum deviations of Eqs. (32) and (33) and corresponding functionals given in Eqs. (34) and (35) leads for  $U/t = 100$ ,  $n = 0.59$ , and  $m \rightarrow 0$  to the one-electron removal spectral-weight distribution plotted in Fig. 6. Such a large-

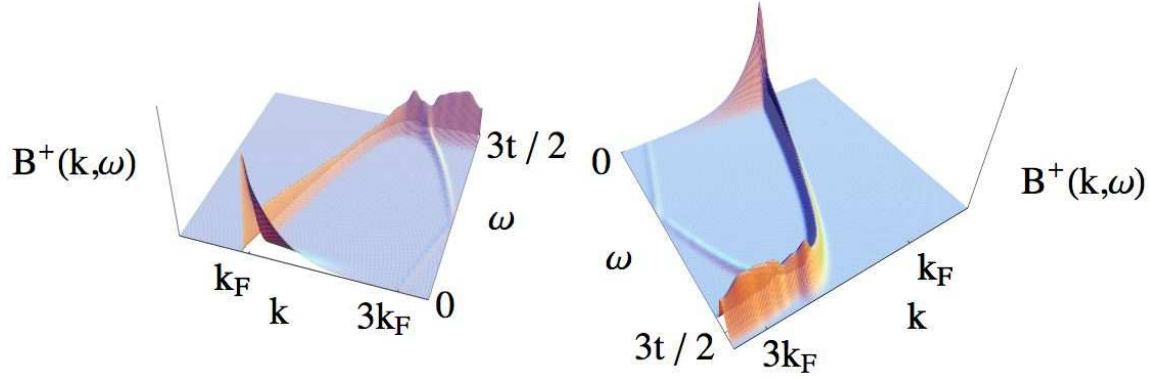


**Figure 12.** Full PDT one-electron addition spectral-weight distribution associated with the  $c0$  and  $s1$  momentum deviations of Eqs. (38) and (39) and corresponding functionals given in Eqs. (40) and (41) for  $U/t = 100$ ,  $n = 0.59$ , and  $m \rightarrow 0$ .

$U/t$  distribution is quite similar to the function  $B(k, \omega)$  plotted in Fig. 1 of Ref. [16] for  $U/t \rightarrow \infty$ . However, the method used in the studies of the latter reference does not apply to finite values of  $U/t$ . The one-electron removal spectral-weight distribution related to the TCNQ spectral features is plotted in Fig. 7 and refers instead to  $U/t = 4.9$ ,  $n = 0.59$ , and  $m \rightarrow 0$ . It is a part of the full one-electron spectral weight distribution plotted in Fig. 1.

Most singular behaviours of the one-electron removal spectral-weight distributions of Figs. 6 and 7 refer to  $c0$  and  $s1$  branch lines whose negative power-law exponents magnitude depends on  $U/t$  and the momentum. These exponents are plotted in Figs. 4 and 5. In turn, the weaker lines connecting in Figs. 2 and 3 the minimum energy points of the two  $c0$  lines are border lines. The singularities of the latter lines correspond instead to the  $U/t$  and momentum independent exponent  $-1/2$ , as given in the general border-line expressions (28) and (29) derived in this paper.

Next let us consider the lower-Hubbard-band one-electron addition spectrum for  $n = 0.59; t = 0.35 \text{ eV}; U/t = 5.61$  from which one derives the TTF related photoemission one-electron removal spectrum for  $n = 1.41; t = 0.35 \text{ eV}; U/t = 5.61$ . Nearly the whole lower-Hubbard-band one-electron addition spectral weight corresponds to the excitations leading to the following deviations from the ground-state  $N_{\alpha\nu}$   $\alpha\nu$  pseudofermion numbers and  $N_{\alpha\nu}^h$   $\alpha\nu$  pseudofermion-hole numbers where  $\alpha\nu = c0, s1$ ,

$$\Delta N_{c0} = -\Delta N_{c0}^h = +1; \quad \Delta N_{s1} = 0; \quad \Delta N_{s1}^h = +1, \quad (36)$$

and with the numbers  $Q_{\alpha\nu}^0/2$  appearing on the right-hand side of Eq. (7) reading,

$$Q_{c0}^0/2 = 0; \quad Q_{s1}^0/2 = \pm\pi/2. \quad (37)$$

If we choose the excitation branches that survive for  $m \rightarrow 0$ , the general deviations are

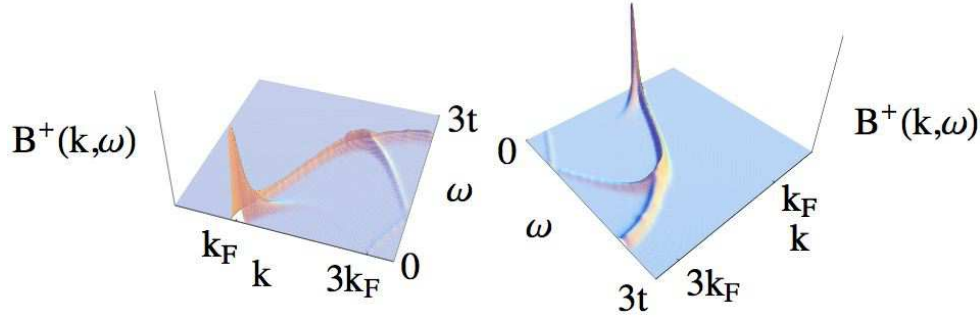


**Figure 13.** The same PDT one-electron addition spectral-weight distribution as in Fig. 8 for the values  $U/t = 5.61$ ,  $n = 0.59$ , and  $m \rightarrow 0$  suitable to the TTF related spectral features.

for bare-momentum continuum values given by,

$$\begin{aligned} \Delta N_{c0}(q) &= \frac{2\pi}{L} \delta(q - q_1); \quad q_1 \in [-2k_F, +\pi] \quad \text{and} \quad q_1 \in [-\pi, +2k_F] \\ \Delta N_{s1}(q) &= -\frac{2\pi}{L} \delta(q - q'_1) + \frac{\pi}{L} \delta(q + k_{F\downarrow}) \\ &\quad + \frac{\pi}{L} \delta(q - k_{F\downarrow}); \quad q'_1 \in [-k_{F\downarrow}, +k_{F\downarrow}], \end{aligned} \quad (38)$$

and thus

$$\begin{aligned} \Delta N_{s1}(q) &= -\frac{2\pi}{L} \delta(q - q'_1) + \frac{\pi}{L} \delta(q - k_F) \\ &\quad + \frac{\pi}{L} \delta(q + k_F); \quad q'_1 \in [-k_F, +k_F] \end{aligned} \quad (39)$$

as  $m \rightarrow 0$  for the initial ground state. Alike for the above one-electron removal case, such deviations and the numbers (37) are used in the general functional  $Q_{\alpha\nu}(q_j)/2$  provided in Eq. (7) and its functional  $Q_{\alpha\nu}^\Phi(q_j)/2$  defined in Eq. (4). One then finds,

$$\begin{aligned} Q_{c0}(q)/2 &= \pi\Phi_{c0,c0}(q, q_1) - \pi\Phi_{c0,s1}(q, q'_1) \\ &\quad + \pi\Phi_{c0,s1}(q, -k_{F\downarrow})/2 + \pi\Phi_{c0,s1}(q, +k_{F\downarrow})/2, \end{aligned} \quad (40)$$

and

$$\begin{aligned} Q_{s1}(q)/2 &= \pm \pi/2 + \pi\Phi_{s1,c0}(q, q_1) - \pi\Phi_{s1,s1}(q, q'_1) \\ &\quad + \pi\Phi_{s1,s1}(q, -k_{F\downarrow})/2 + \pi\Phi_{s1,s1}(q, +k_{F\downarrow})/2, \end{aligned} \quad (41)$$

respectively.

The creation of the  $c0$  pseudofermion and  $s1$  pseudofermion hole refers for  $U/t = 100$ ,  $n = 0.59$ , and  $m \rightarrow 0$  to a finite spectral-weight distribution in the region of the  $(k, \omega)$  plane shown in Fig. 8. The corresponding lines associated with potential branch lines and border lines are also plotted. In Fig. 9 the same finite spectral-weight region is shown for the  $U/t = 5.61$ ,  $n = 0.59$ , and  $m \rightarrow 0$  values suitable to the TTF

related spectral features. The border line connecting the maximum energy point of the  $c0$ -branch line at momentum  $2k_F$  with the maximum energy point of the finite spectral-weight distribution at momentum  $\pi$  has in Fig. 8  $v_{c0}(q) = v_{s1}(q') \approx 0$ . Upon decreasing  $U/t$  to the value  $U/t = 5.61$  suitable to the TTF related spectral features of Fig. 1 that border line acquires a curvature, as shown in Fig. 9. Such a curvature and corresponding value of  $U/t$  are those behind the agreement achieved in Ref. [4] between the PDT predictions and the photoemission spectral features of TTF-TCNQ.

The  $c0$  branch lines of the weight distributions of Figs. 8 and 9 run between the excitation momenta  $k_F$  and  $\pi$  and between  $3k_F$  and  $\pi$ , respectively. In turn, the maximum extension of the  $s1$  branch line is achieved for large values of  $U/t$  when it runs from  $k_F$  to near  $3k_F$ . The corresponding power-law momentum dependent exponents are plotted in Fig. 10 for  $n = 0.59$ ,  $m \rightarrow 0$ , and several values of  $U/t$ . While the  $c0$  branch lines exponents are negative, the  $s1$  branch line exponent is negative for momenta smaller than approximately  $k_F$  and  $2k_F$  for  $U/t = 5.61$  and  $U/t = 100$ , respectively. Again in order to illustrate the evolution of the spectral features upon varying the parameters, the same exponents as in Fig. 10 are plotted in Fig. 11 as a function of momentum for  $U/t = 10$ ,  $m \rightarrow 0$ , and several values of  $n$ .

The general PDT spectral-function expressions provided in this paper and in Ref. [2] lead for  $U/t = 100$ ,  $n = 0.59$ , and  $m \rightarrow 0$  and the specific  $c0$  and  $s1$  momentum deviations of Eqs. (38) and (39) and corresponding functionals provided in Eqs. (40) and (41) to the one-electron addition spectral-weight distribution plotted in Fig. 12. The large- $U/t$  distribution plotted in that figure is quite similar to the function  $A(k, \omega)$  plotted in Fig. 1 of Ref. [16] for  $U/t \rightarrow \infty$ . The one-electron addition spectral-weight distribution related to the TTF spectral features is plotted in Fig. 13 and refers instead to  $U/t = 5.61$ ,  $n = 0.59$ , and  $m \rightarrow 0$ . After a straightforward particle-hole transformation, the latter distribution leads to the one-electron removal spectral-weight distribution suitable to the TTF related spectral features. The latter corresponds to  $U/t = 5.61$ ,  $n = 1.41$ , and  $m \rightarrow 0$  and is part of the full one-electron removal spectral-weight distribution plotted in Fig. 1.

Most singular behaviours of the one-electron addition spectral-weight distributions of Figs. 12 and 13 correspond to  $c0$  and  $s1$  branch lines whose negative power-law exponents are dependent on the  $U/t$  and momentum values. These exponents are plotted in Figs. 10 and 11 and the power-law singularities occur for the momenta where they are negative. In turn, the line connecting in Figs. 8 and 9 the maximum energy point of the  $c0$ -branch line at momentum  $2k_F$  with the maximum energy point of the finite spectral-weight distribution at momentum  $\pi$  is a border line. The singularities at the latter line correspond to the  $U/t$  and momentum independent exponent  $-1/2$  and near it the line shape is of the general form provided in expressions (28) and (29).

The four functionals  $2\Delta_{\alpha\nu}^t$  where  $\alpha\nu = c0, s1$  and  $t = \pm 1$  given in Eq. (10) are in the case of the one-electron excitations behind the spectral-weight distribution plotted in Fig. 1 fully controlled by the functionals provided in Eqs. (34) and (35) for  $U/t = 4.90$ ,  $n = 0.59$ , and  $m \rightarrow 0$  for the TCNQ related spectral features and in Eqs. (40) and

(41) for  $U/t = 5.61$ ,  $n = 0.59$ , and  $m \rightarrow 0$  for the TTF related spectral features. Since the magnitude of the latter functionals is a function of two momenta  $q_1$  and  $q'_1$  of the deviations of Eqs. (32) and (33) or Eqs. (38) and (39) belonging to the  $c0$  and  $s1$  band, respectively, it is different for each point of the  $(k, \omega)$  plane. Moreover, for some of the latter points there are contributions from more than one pair of momenta of  $q_1$  and  $q'_1$ .

We emphasize that depending on whether none, one, or two of the two above momenta  $q_1$  and  $q'_1$  is or are Fermi points, the corresponding functionals  $2\Delta_{\alpha\nu}^{\iota}$  have different form and the excitation contributes to line shapes described by the expressions provided in Eqs. (66), (70), and (68) of Ref. [2], respectively. All such expressions involve the pre-factor function  $F_0(z)$  given in Eqs. (A.1)-(A.7) of Appendix A. The expressions provided in these equations are a generalization of the pre-factor function  $F_0(z)$  provided in Eq. (62) of Ref. [2]. The latter applies when the four functionals  $2\Delta_{\alpha\nu}^{\iota}$  where  $\alpha\nu = c0, s1$  and  $\iota = \pm 1$  are finite. However, in the limit  $m \rightarrow 0$  that the spectral-weight distributions studied in this paper refer to one must use in the general expressions provided in Eqs. (66), (70), and (68) of Ref. [2] the pre-factor function  $F_0(z)$  of Eqs. (A.1)-(A.7) of Appendix A.

Note that the above mentioned general expressions provided in Eqs. (68) and (70) of Ref. [2] describe the line shape near well-define points and lines in the  $(k, \omega)$  plane, respectively. When the corresponding exponents are negative, such spectral features refer to the point and branch-line singularities of the weight distributions plotted in Figs. 1, 6, 7, 12, and 13. In turn, the only type of singularity occurring within the line shape described by the above mentioned general expression provided in Eq. (66) of Ref. [2] is that associated with the border lines studied in the previous section. The corresponding expressions (28) and (29) refer to the vicinity of such border lines.

The complementary studies of Ref. [18] provide the specific expressions of the four functionals  $2\Delta_{\alpha\nu}^{\iota}$  where  $\alpha\nu = c0, s1$  and  $\iota = \pm 1$  given in Eq. (10) for each of the point and branch-line singularities of the TCNQ related one-electron removal spectral features. The functionals given in Eqs. (40) and (41) are the basis of the derivation of similar expressions for the TTF related spectral features. Those are straightforwardly derived by choosing particular pairs of momentum values  $q_1$  and  $q'_1$  in the  $c0$  and  $s1$  momentum deviations of Eqs. (38) and (39), respectively. As discussed above, when such choices involve none, one, or both such momentum pairs being a  $c0$  or  $s1$  Fermi point, the corresponding four functionals  $2\Delta_{\alpha\nu}^{\iota}$  have different forms and the excitation contributes to line shapes described by the expressions provided in Eqs. (66), (70), and (68) of Ref. [2] for the two-dimensional weight distribution, vicinity of branch lines, and vicinity of singular points, respectively.

Finally, in Fig. 14 we plot the theoretical lines corresponding to the sharpest spectral features considered in Fig. 1 but omit the corresponding detailed spectral-weight distribution over the  $(k, \omega)$ -plane provided in that figure. The figure also displays the experimental dispersions in the electron removal spectrum of TTF-TCNQ as measured by ARPES in Ref. [9]. The border line connecting the maximum energy point of the  $c0$ -branch line at momentum  $2k_F$  with the maximum energy point of the

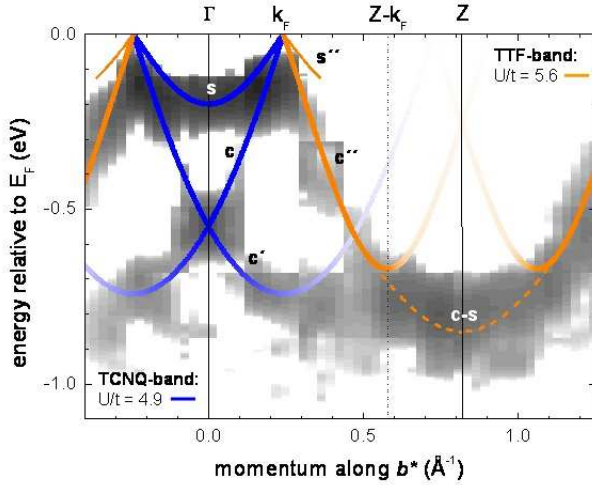


**Figure 14.** Experimental peak dispersions (grey scale) obtained by ARPES on TTF-TCNQ along the easy-transport axis as given in Fig. 7 of Ref. [9] and matching theoretical branch and border lines. (The Z-point corresponds to the momentum  $k = \pi$ .) The corresponding detailed theoretical spectral-weight distributions over the whole  $(k, \omega)$ -plane are plotted above in Fig. 1. While the theoretical charge- $c''$  and spin- $s''$  branch lines and  $c-s$  border line refer upon the particle-hole transformation to the TTF related spectral features of Figs. 9 and 13, the charge- $c$ , spin- $s$ , and charge- $c'$  branch lines correspond to the TCNQ related dispersions of Figs. 3 and 7.

finite spectral-weight distribution at momentum  $\pi$  in Fig. 9 leads upon the particle-hole transformation to that called  $c-s$  line in Fig. 14. In turn the border line connecting the minimum energy points of the two  $c_0$  lines of Fig. 3 associated with the TCNQ related spectral features is not marked in Fig. 14, yet the corresponding experimental spectral weight is clearly visible.

## 5. DISCUSSION AND CONCLUDING REMARKS

In this paper we have generalized the closed-form analytical expressions for the finite-energy one- and two-electron spectral-weight distributions of a 1D correlated metal with on-site electronic repulsion introduced in Ref. [2] to all electronic densities of the metallic phase and zero spin density. Moreover, we have studied the particular form of the expressions derived here for the processes contributing to the one-electron spectral-weight distributions related to the TTF and TCNQ stacks of molecules, respectively, in the quasi-1D organic compound TTF-TCNQ investigated in Ref. [4]. The corresponding full theoretical one-electron spectral-weight distribution plotted in Fig. 1 agrees quantitatively for the whole experimental energy bandwidth with the observed one-electron spectral features shown in Fig. 14.

Other applications of our finite-energy spectral-weight-distribution expressions to several materials, correlated quantum systems, and spectral functions are in progress.

This includes the use of our theoretical results in the two-atom spectral-weight distributions measured in 1D optical lattices. Such studies also involve the Hubbard model but with the electrons replaced by fermionic spin-1/2 atoms. While for the one-electron features the branch lines play the major role, in the case of two-electron spectral functions such as the charge dynamical structure factor the two-pseudofermion spectral features of the form given in Eq. (66) of Ref. [2] lead to the main contributions. Generalization of that equation to all electronic densities of the metallic phase and to zero spin density involves the use of the following expression,

$$\begin{aligned}
 B_{\mathcal{N}}^l(k, \omega) \approx & \frac{1}{\pi C_c C_s} \left[ \int_{-1/v_{\bar{a}\bar{v}}}^{+1/v_{\bar{a}\bar{v}}} dz F_0(z) \right] \left( \frac{\Omega}{4\pi\sqrt{v_{c0} v_{s1}}} \right)^{\zeta_0(q', q'')} \\
 & \times \frac{\sqrt{v_{c0} v_{s1}}}{\zeta_0(q', q'') |v_{\alpha'\nu'}(q') - v_{\alpha''\nu''}(q'')|} ; \quad l = \pm 1, \quad (42)
 \end{aligned}$$

with the pre-factor function  $F_0(z)$  given by the expressions (A.1)-(A.7) of Appendix A introduced in this paper. Alike in Eq. (28), here  $q'$  and  $q''$  stand for the bare-momentum values of the created  $\alpha'\nu'$  and  $\alpha''\nu''$  pseudofermions or holes, respectively. Indeed, the singular border-line function (28) is a particular case of the general function provided in Eq. (42), which can be obtained by considering that  $v_{\alpha'\nu'}(q') = v_{\alpha''\nu''}(q'')$  in the latter equation.

For finite values of  $U/t$  the dominant term of the two-electron spectral functions is often of the general form given in Eq. (42). However, it can also occur that for intermediate values of  $U/t$  such functions are the sum of two or three dominant functions of the general form (42). The main contributions correspond to the two created objects being such that (i)  $\alpha'\nu' = c0$  and  $\alpha''\nu'' = s1$ , (ii)  $\alpha'\nu' = \alpha''\nu'' = c0$ , and (iii)  $\alpha'\nu' = \alpha''\nu'' = s1$ . The relative importance of the functions (i)-(iii) and whether the two created objects are pseudofermions and/or pseudofermion holes depends on the specific two-electron spectral function under consideration. Our general expressions (A.1)-(A.7) of Appendix A for the pre-factor function  $F_0(z)$  appearing on the right-hand side of Eq. (42) allows the evaluation of all two-electron spectral-weight distributions for initial ground states with zero spin density, which in many situations is the case of physical interest. The branch lines and other spectral features also contribute to the two-electron spectral-weight distributions, yet the dominant contributions are of the general form given in Eq. (42).

For instance, the preliminary results of Ref. [20] consider both one- and two-electron spectral features, profits from the PDT for the one-chain problem, are consistent with the phase diagram observed in the  $(\text{TMTTF})_2\text{X}$  and  $(\text{TMTSF})_2\text{X}$  series of organic compounds, and explain the absence of superconductive phases in TTF-TCNQ. The studies of that reference combine the PDT for several one- and two-electron spectral functions with a Renormalization Group analysis to study the instabilities of a system of weakly coupled Hubbard chains. For low values of the onsite repulsion  $U$  and of the doping  $\delta = (1 - n)$ , the leading instability is towards a superconducting state. The process includes excited states above a small correlation pseudogap. Similar features

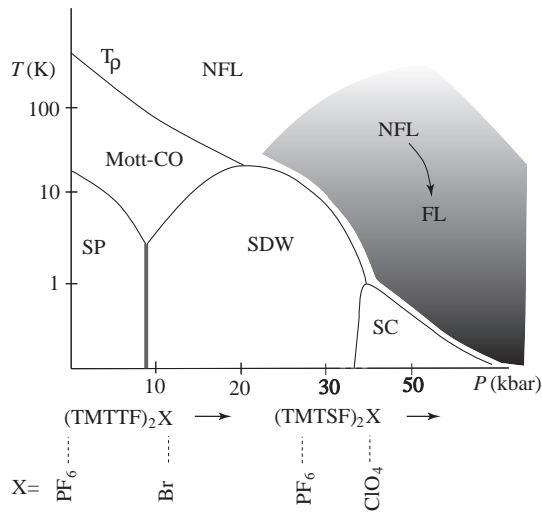


**Figure 15.** Temperature-pressure phase diagram of the  $(\text{TMTTF})_2\text{X}$  and  $(\text{TMTSF})_2\text{X}$  series of compounds. It includes non-Fermi liquid (NFL), insulating Mott-Hubbard (Mott-CO), spin-density-wave (SDW), spin-Peierls, Fermi-liquid (FL), and superconducting (SC) phases.

appear in extended Hubbard models in the vicinity of commensurate fillings. The theoretical predictions of such studies are consistent with the phase diagram observed in the  $(\text{TMTTF})_2\text{X}$  and  $(\text{TMTSF})_2\text{X}$  series of organic compounds represented in Fig. 15. From the results of Ref. [20] one can infer that the low-temperature phase of the coupled-chain system will show long-range superconducting order. However, the precise nature of this phase, and the symmetry of the order parameter is dependent on the arrangement of the chains within the material. The investigations of Ref. [20] use the exponents obtained from the PDT for the one-chain problem and confirm that in 1D non-Fermi liquids weak inter-chain hopping can induce superconductivity. At low temperature these materials show a spin-Peierls or spin-density-wave phase. Under pressure, the  $(\text{TMTSF})_2\text{X}$  compounds are driven to a superconducting phase, which is removed again if one further increases the pressure.

In addition to the finite-energy spectral features of the organic compound TTF-TCNQ [4] and the preliminary studies of Ref. [20] on the  $(\text{TMTTF})_2\text{X}$  and  $(\text{TMTSF})_2\text{X}$  series of organic compounds, the general spectral-function expressions derived in this paper will be used elsewhere in the study of specific one- and two-electron spectral functions and its quantitative application to the unusual spectral properties of other low-dimensional materials and systems. While the studies of this paper considered the 1D Hubbard model, which describes successfully some of the exotic properties observed in low-dimensional materials [9, 18, 19, 20], our results are of general nature for many integrable interacting problems [1] and therefore have wide applicability.

We thank Pedro D. Sacramento for stimulating discussions and the support of ESF Science Program INSTANS, European Union Contract 12881 (NEST), FCT grants SFRH/BD/6930/2001, POCTI/FIS/58133/2004, and PTDC/FIS/64926/2006 and and

OTKA grant T049607.

### Appendix A. The pre-factor function $F_0(z)$

In this Appendix a set of alternative expressions for the pre-factor function  $F_0(z)$  on the right-hand side of Eq. (25) derived by use of Eqs. (19), (20), (21), (23), and (25) according to the values of the two parameters  $2\Delta_{\alpha\nu}^{\pm 1}$  and two parameters  $2\Delta_{\bar{\alpha}\bar{\nu}}^{\pm 1}$  are given.

(i) When the four parameters  $2\Delta_{\alpha\nu}^{\pm 1}$  where  $\alpha\nu = c0, s1$  and  $\iota = \pm 1$  are finite we find,

$$\begin{aligned}
 F_0(z) &= 2D_0 \sqrt{\frac{v_{\bar{\alpha}\bar{\nu}}}{v_{\alpha\nu}}} \int_0^1 dx \int_{-1}^{+1} dy \\
 &\times \prod_{\iota'=\pm 1} \frac{\Theta\left(1 - x + \text{sgn}(z) \iota' \left[v_{\bar{\alpha}\bar{\nu}}|z| - \frac{v_{\bar{\alpha}\bar{\nu}}}{v_{\alpha\nu}} y\right]\right)}{\Gamma(2\Delta_{\bar{\alpha}\bar{\nu}}^{\iota'})} \\
 &\times \frac{\Theta\left(x + \text{sgn}(z) \iota' y\right)}{\Gamma(2\Delta_{\alpha\nu}^{\iota'})} \\
 &\times \left(\sqrt{\frac{v_{\alpha\nu}}{v_{\bar{\alpha}\bar{\nu}}}} \left[1 - x + \text{sgn}(z) \iota' \left[v_{\bar{\alpha}\bar{\nu}}|z| - \frac{v_{\bar{\alpha}\bar{\nu}}}{v_{\alpha\nu}} y\right]\right]\right)^{2\Delta_{\bar{\alpha}\bar{\nu}}^{\iota'} - 1} \\
 &\times \left(\sqrt{\frac{v_{\bar{\alpha}\bar{\nu}}}{v_{\alpha\nu}}} \left[x + \text{sgn}(z) \iota' y\right]\right)^{2\Delta_{\alpha\nu}^{\iota'} - 1}. \tag{A.1}
 \end{aligned}$$

(ii) When  $2\Delta_{\bar{\alpha}\bar{\nu}}^{-\bar{\iota}} = 0$  and the remaining three parameters are finite,

$$\begin{aligned}
 F_0(z) &= 2D_0 \frac{v_{\bar{\alpha}\bar{\nu}}}{v_{\alpha\nu}} \int_{-1}^{+1} dy \\
 &\times \frac{\Theta\left(\bar{\iota} [\text{sgn}(z)y - v_{\alpha\nu} \left(z - \frac{\bar{\iota}}{v_{\bar{\alpha}\bar{\nu}}}\right)]\right) \Theta\left(\bar{\iota} [zv_{\alpha\nu} - \text{sgn}(z)y]\right)}{\Gamma(2\Delta_{\bar{\alpha}\bar{\nu}}^{\bar{\iota}})} \\
 &\times \left(\sqrt{\frac{v_{\alpha\nu}}{v_{\bar{\alpha}\bar{\nu}}}} 2\bar{\iota} \left[z - \text{sgn}(z) \frac{y}{v_{\alpha\nu}}\right] v_{\bar{\alpha}\bar{\nu}}\right)^{2\Delta_{\bar{\alpha}\bar{\nu}}^{\bar{\iota}} - 1} \\
 &\times \prod_{\iota'=\pm 1} \frac{\Theta\left(1 + \text{sgn}(z) \left[\iota' + \bar{\iota} \frac{v_{\bar{\alpha}\bar{\nu}}}{v_{\alpha\nu}}\right] y - \bar{\iota} v_{\bar{\alpha}\bar{\nu}} z\right)}{\Gamma(2\Delta_{\alpha\nu}^{\iota'})} \\
 &\times \left(\sqrt{\frac{v_{\bar{\alpha}\bar{\nu}}}{v_{\alpha\nu}}} \left[1 + \text{sgn}(z) \left[\iota' + \bar{\iota} \frac{v_{\bar{\alpha}\bar{\nu}}}{v_{\alpha\nu}}\right] y - \bar{\iota} v_{\bar{\alpha}\bar{\nu}} z\right]\right)^{2\Delta_{\alpha\nu}^{\iota'} - 1}. \tag{A.2}
 \end{aligned}$$

(iii) When  $2\Delta_{\alpha\nu}^{-\iota} = 0$  and the remaining three parameters are finite,

$$\begin{aligned}
 F_0(z) &= 2D_0 \int_{-1}^{+1} dy \frac{\Theta\left(\iota \text{sgn}(z)y\right)}{\Gamma(2\Delta_{\alpha\nu}^{\iota})} \left(\sqrt{\frac{v_{\bar{\alpha}\bar{\nu}}}{v_{\alpha\nu}}} \iota \text{sgn}(z) 2y\right)^{2\Delta_{\alpha\nu}^{\iota} - 1} \\
 &\times \prod_{\iota'=\pm 1} \frac{\Theta\left(1 - \text{sgn}(z) \left[\iota + \bar{\iota}' \frac{v_{\bar{\alpha}\bar{\nu}}}{v_{\alpha\nu}}\right] y + \bar{\iota}' v_{\bar{\alpha}\bar{\nu}} z\right)}{\Gamma(2\Delta_{\bar{\alpha}\bar{\nu}}^{\bar{\iota}'})}
 \end{aligned}$$

$$\times \left( \sqrt{\frac{v_{\alpha\nu}}{v_{\bar{\alpha}\bar{\nu}}}} \left[ 1 - \text{sgn}(z) \left[ \iota + \bar{\iota}' \frac{v_{\bar{\alpha}\bar{\nu}}}{v_{\alpha\nu}} \right] y + \bar{\iota}' v_{\bar{\alpha}\bar{\nu}} z \right] \right)^{2\Delta'_{\bar{\alpha}\bar{\nu}}-1}. \quad (\text{A.3})$$

(iv) When both  $2\Delta'_{\bar{\alpha}\bar{\nu}} = 0$  and the remaining two parameters are finite,

$$F_0(z) = D_0 \sqrt{\frac{v_{\bar{\alpha}\bar{\nu}}}{v_{\alpha\nu}}} \Theta\left(\frac{1}{v_{\alpha\nu}} - |z|\right) \times \prod_{\iota'=\pm 1} \frac{1}{\Gamma(2\Delta'_{\alpha\nu})} \left( \sqrt{\frac{v_{\bar{\alpha}\bar{\nu}}}{v_{\alpha\nu}}} \left[ 1 + \iota' v_{\alpha\nu} z \right] \right)^{2\Delta'_{\alpha\nu}-1}. \quad (\text{A.4})$$

(v) When both  $2\Delta'_{\alpha\nu} = 0$  and the remaining two parameters are finite,

$$F_0(z) = D_0 \sqrt{\frac{v_{\alpha\nu}}{v_{\bar{\alpha}\bar{\nu}}}} \prod_{\bar{\iota}'=\pm 1} \frac{\Theta\left(\frac{1}{v_{\bar{\alpha}\bar{\nu}}} - \bar{\iota}' z\right)}{\Gamma(2\Delta'_{\bar{\alpha}\bar{\nu}})} \left( \sqrt{\frac{v_{\alpha\nu}}{v_{\bar{\alpha}\bar{\nu}}}} \left[ 1 - \bar{\iota}' v_{\bar{\alpha}\bar{\nu}} z \right] \right)^{2\Delta'_{\bar{\alpha}\bar{\nu}}-1} = 0. \quad (\text{A.5})$$

(vi) When  $2\Delta_{\alpha\nu}^{-\iota} = 2\Delta_{\bar{\alpha}\bar{\nu}}^{-\bar{\iota}} = 0$  and the remaining two parameters are finite,

$$F_0(z) = \frac{2D_0}{\sqrt{v_{\alpha\nu}v_{\bar{\alpha}\bar{\nu}}}} \left( \frac{v_{\alpha\nu} - \iota\bar{\iota}v_{\bar{\alpha}\bar{\nu}}}{v_{\alpha\nu}v_{\bar{\alpha}\bar{\nu}}} \right)^{1-\zeta_0} \times \frac{\Theta\left(\bar{\iota}\left[z - \frac{\iota}{v_{\alpha\nu}}\right]\right) \Theta\left(\frac{1}{v_{\bar{\alpha}\bar{\nu}}} - \bar{\iota}z\right)}{\Gamma(2\Delta_{\bar{\alpha}\bar{\nu}}^{\bar{\iota}}) \Gamma(2\Delta_{\alpha\nu}^{\iota})} \times \left( 2\sqrt{\frac{v_{\alpha\nu}}{v_{\bar{\alpha}\bar{\nu}}}} \bar{\iota}\left[z - \frac{\iota}{v_{\alpha\nu}}\right] \right)^{2\Delta_{\bar{\alpha}\bar{\nu}}^{\bar{\iota}}-1} \left( 2\sqrt{\frac{v_{\bar{\alpha}\bar{\nu}}}{v_{\alpha\nu}}} \left[ \frac{1}{v_{\bar{\alpha}\bar{\nu}}} - \bar{\iota}z \right] \right)^{2\Delta_{\alpha\nu}^{\iota}-1}. \quad (\text{A.6})$$

(vii) When both  $2\Delta_{\alpha\nu}^{\iota} > 0$  (and  $2\Delta_{\bar{\alpha}\bar{\nu}}^{\bar{\iota}} > 0$ ) and the remaining three parameters vanish,

$$F_0(z) = \frac{D_0}{v_{\alpha\nu}\Gamma(2\Delta_{\alpha\nu}^{\iota})} \left( 2\sqrt{\frac{v_{\bar{\alpha}\bar{\nu}}}{v_{\alpha\nu}}} \right)^{2\Delta_{\alpha\nu}^{\iota}-1} \delta\left(z - \frac{\iota}{v_{\alpha\nu}}\right), \quad (\text{A.7})$$

(and a similar expression with  $\alpha\nu, \iota$ , and  $\bar{\alpha}\bar{\nu}$  replaced by  $\bar{\alpha}\bar{\nu}, \bar{\iota}$ , and  $\alpha\nu$ , respectively).

- [1] Voit J 1995 *Rep. Prog. Phys.* **58** 977 and references therein.
- [2] Carmelo JMP, Penc K and Bozi D 2005 *Nucl. Phys. B* **725** 421; 2006 *Nucl. Phys. B (erratum)* **737** 351.
- [3] Carmelo JMP and Penc K 2006 *Eur. Phys. J. B* **51** 477.
- [4] Bozi D, Carmelo JMP, Penc K and Sacramento PD 2008 *J. Phys.: Cond. Mat.* **20** 022205.
- [5] Pereira RG, Sirker J, Caux JS, Hagemans R, Maillet JM, White SR and Affleck I 2006 *Phys. Rev. Lett.* **96** 257202; Pereira RG, White SR and Affleck I 2008 *Phys. Rev. Lett.* **100** 027206; White SR and Affleck I 2008 *Phys. Rev. B* **77** 134437.
- [6] Pustilnik M, Khodas M, Kamenev A and Glazman LI 2006 *Phys. Rev. Lett.* **96** 196405; Khodas M, Pustilnik M, Kamenev A and Glazman LI 2007 *Phys. Rev. Lett.* **99** 110405; Khodas M, Pustilnik M, Kamenev A and Glazman LI 2007 *Phys. Rev. B* **76** 155402; Imambekov A and Glazman LI 2008 *Phys. Rev. Lett.* **100** 206805.
- [7] Carmelo JMP, Martelo LM and Penc K 2006 *Nucl. Phys. B* **737** 237; Carmelo JMP and Penc K 2006 *Phys. Rev. B* **73** 113112.
- [8] Zwick F, Jérôme D, Margaritondo G, Onellion M, Voit J and Grioni M 1998 *Phys. Rev. Lett.* **81** 2974; Claessen R, Sing M, Schwingenschlögl U, Blaha P, Dressel M and Jacobsen CS 2002 *Phys. Rev. Lett.* **88** 096402.
- [9] Sing M, Schwingenschlögl U, Claessen R, Blaha P, Carmelo JMP, Martelo LM, Sacramento PD, Dressel M and Jacobsen CS 2003 *Phys. Rev. B* **68** 125111.

- [10] Jaksch D and Zoller P 2005 *Ann. Phys.* **315** 52; Liu Xia-Ji, Drummond Peter D and Hu Hui 2005 *Phys. Rev. Lett.* **94** 136406.
- [11] Lieb Elliot H and Wu FY 1968 *Phys. Rev. Lett.* **20** 1445; Martins MJ and Ramos PB 1998 *Nucl. Phys. B* **522** 413.
- [12] Takahashi M 1972 *Prog. Theor. Phys.* **47** 69.
- [13] Heilmann OJ and Lieb EH 1971 *Ann. N. Y. Acad. Sci.* **172** 583; Yang CN 1989 *Phys. Rev. Lett.* **63** 2144.
- [14] Carmelo JMP, Román JM and Penc K 2004 *Nucl. Phys. B* **683** 387.
- [15] Carmelo JMP and Sacramento PD 2003 *Phys. Rev. B* **68** 085104.
- [16] Penc K, Hallberg K, Mila F and Shiba H 1996 *Phys. Rev. Lett.* **77** 1390.
- [17] Penc K, Hallberg K, Mila F and Shiba H 1997 *Phys. Rev. B* **55** 15 475.
- [18] Carmelo JMP, Penc K, Sacramento PD, Sing M and Claessen R 2006 *J. Phys.: Cond. Matt.* **18** 5191.
- [19] Benthien H, Gebhard F and Jeckelmann E 2004 *Phys. Rev. Lett.* **92** 256401.
- [20] Carmelo JMP, Guinea F, Penc K and Sacramento PD 2004 *Europhys. Lett.* **68** 839.
- [21] Belavin AA, Polyakov AM and Zamolodchikov AB 1984 *Nucl. Phys. B* **241** 333.
- [22] Schulz HJ 1990 *Phys. Rev. Lett.* **64** 2831; Carmelo JMP, Castro Neto AH and Campbell DK 1994 *Phys. Rev. Lett.* **73** 926; *ibid.* 1994 *Phys. Rev. B* **50** 3683.
- [23] Carmelo JMP 2005 *J. Phys.: Cond. Matt.* **17** 5517.
- [24] Jordan P and Wigner E 1928 *Z. Phys.* **47** 631.
- [25] While the first expression provided in Eq. (56) of Ref. [2] is correct, there is a misprint in its second expression. It must be multiplied by 2 what gives our expressions of Eq. (19). Such a misprint became an error that propagated to expression (62) of that reference which must be multiplied by 4. That gives our expression (A.1) of Appendix A for  $v_{c0} > v_{s1}$ . Furthermore, it propagated to Ref. [7] so that the pre-factor given in Eq. (50) of the latter reference must also be multiplied by 4. Finally, while the exponent of expression (73) of Ref. [2] is correct, the prefactor is a poor approximation.